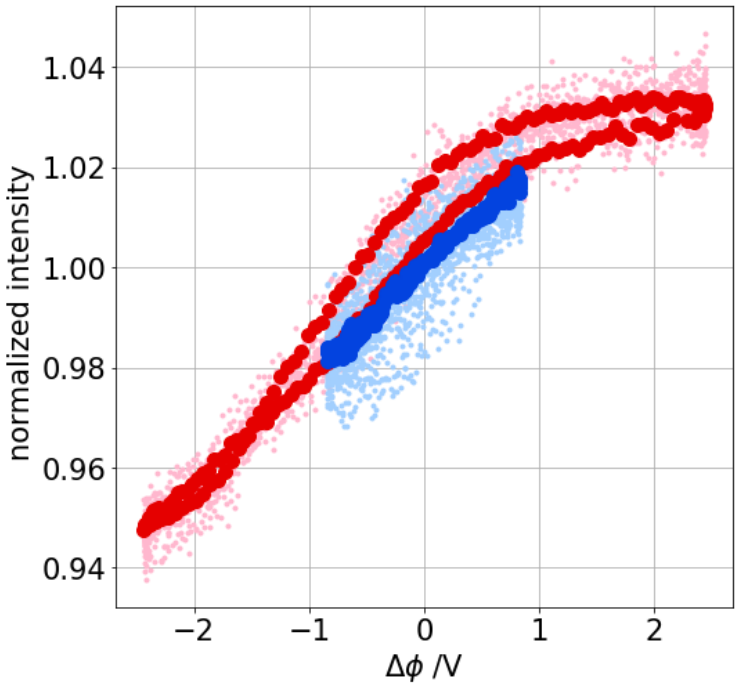

Potentiodynamic Optical Contrast

December 16, 2019

Kevin Namink

Abstract

Charged solid structures in the presence of an electrolyte form a electric double layer (EDL). The EDL determines the electrochemical activity and influences the electrical and optical polarizability of these structures. Building a microscope capable of detecting the influence of the EDL on the optical polarizability of particles would assist in research on the EDL and potentiodynamic reactions. I report on the capabilities and workings of our home-build total internal reflection microscope with enhanced stability and conductive flowcell samples. Results include the experimentally demonstration that with this custom total internal reflection microscope we can detect restructuring of the EDL at the nanoscale. The temporal and spatial characterization of the scattering signal demonstrate that the potentiodynamic optical contrast (PDOC) is proportional to the accumulated charge of polarizable ions at the interface and its time derivative represents the nanoscale ionic current.

Contents

1 Introduction **3**

2 Theory **4**
2.1 Electrical double layer . . . 4
2.2 Polarizability . . . 4
2.3 Refractive index of solutions . . . 5
2.4 Rayleigh scattering . . . 5
2.5 Fourier transforms . . . 6
2.6 Potential induced reactions . . . 6
2.7 Cyclic voltammetry . . . 6
2.8 Prediction on potentiodynamic optical scattering . . . 7

3 Microscopy **9**
3.1 Dark field microscopy . . . 9
3.2 Total internal reflection microscopy . . . 10
3.3 PID controlled stability . . . 10

4 Materials and methods **11**
4.1 Experimental setup . . . 11
4.2 Optics . . . 11
4.3 QPD controlled focus . . . 12
4.4 Electronics . . . 13
4.5 Wave generation . . . 13
4.6 A transparent electrode . . . 13
4.7 Sample . . . 14
4.8 UUTrack software . . . 15
4.9 Method . . . 16

5 Calibration **18**
5.1 Magnification of setup . . . 18
5.2 Identifying particles . . . 18
5.2.1 Getting particles to land . . . 20
5.2.2 Identifying particle landings . . . 20
5.3 Long term drift . . . 22
5.4 Short term drift . . . 23

6 Data processing **25**
6.1 Particle selection . . . 25
6.2 Drift correction . . . 25
6.3 Cycle averaging . . . 26
6.4 Filtering anomalies . . . 27
6.5 Possible graphs . . . 27

7 Results **29**
7.1 Intensity change proportional to polarizability . . . 29
7.2 Deposited chromium particles . . . 32
7.3 Varied offset potentiodynamic optical contrast . . . 34

8 Discussion **38**
8.1 Intensity change due to the electric double layer . . . 38
8.2 Deposited chromium particles . . . 38

8.3 Varied offset potentiodynamic optical contrast . . . 38
8.4 Compared to other potentiodynamic techniques . . . 39
8.5 Outlook . . . 39

A List of materials **42**

B UUTrack code **44**
B.1 Data generated by UUTrack . . . 44
B.2 UUTrack dependencies . . . 44
B.3 /PDSMGUI . . . 45
B.4 /UUTrack . . . 45
B.5 /UUTrack/Controller/devices . . . 45
B.6 /UUTrack/Model . . . 45
B.7 /UUTrack/Model/Cameras . . . 46
B.8 /UUTrack/View . . . 46
B.9 /UUTrack/View/Monitor . . . 46

C Data analysis code **48**
C.1 DFSM.py . . . 48
C.2 new analysis file.py . . . 48
C.3 LandingCheck.py . . . 48

1 Introduction

I will be using total internal reflection microscopy, section 3.2, to look at very small particles, so small the light they scatter under total internal reflection microscopy is influenced by chemical reactions on their surface[1]. Using total internal reflection microscopy I will explore the effect of an electrical potential on a particle in a solvent. When the polarization, figure 1, of a particle under an electrical potential changes we can record this at millisecond scale time intervals. With this time-resolution we will follow the changes to our particles during potential varying measurements which can tell us more about the dynamics of particles under a potential, this technique is similar to cyclic voltammetry, section 2.7.

Being able to visually study reactions of single particles under an electrical potential is very exciting because they could be different than bulk properties [2] and potentiodynamics with spatial resolution of a few nanometers has not been studied in a micrometer length scale area at the same time [3]. In a non-homogeneous mixture of particles it could also be possible to measure the different species individually and concurrently.

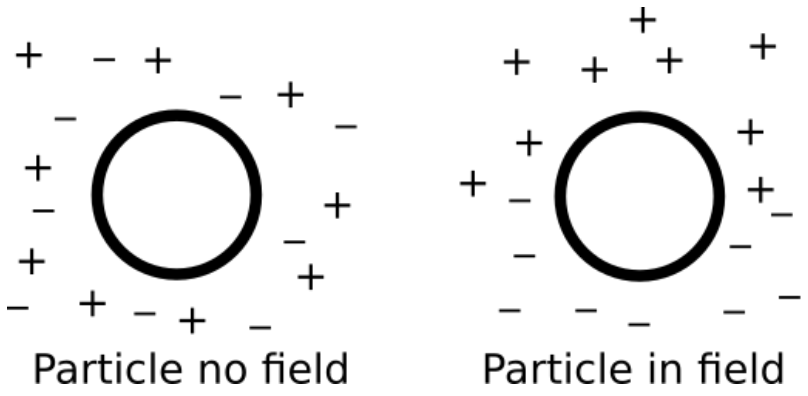

Figure 1: A particle with surrounding charges without and within an electric field. When there is a field over the particle the charges are no longer evenly distributed around the particle; negative charges are attracted to the positive side of the field and the other way around.

My first work after being accepted as master student was to finish the setup and be able to use it to gather data using the "UUTrack" software developed in the group, section 4.8. To finish the setup it was necessary for stability to be improved by using an extra sensor to create a feedback loop, section 4.3. Implementing UUTrack meant learning to understand its code and adding new features to it until it satisfied our needs.

When the setup was capable of doing measurements, the next thing was to finally find out if the predicted (small) variation caused by applying potential was optically visible. After trying some measurements I can spoil for you that we were happy that we could actually see this effect even while measuring.

This thesis contains a conventional hypothesis, at the end of section 2.8, and all the things associated with it, but a large portion of the contents of this thesis is on the work I did to eventually enable us to answer this hypothesis. This enabling work includes details and reasoning behind the workings of the setup, the data analysis and other measurements.

I use the data of many experiment to argue for three main results. First a result that should convince you that the technique developed works. Second a result to show the technique does indeed have the advantage of having useful, relatively large, spatial resolution. And third a result that explores a different technique of doing measurements. With these results I finally argue for this techniques usefulness.

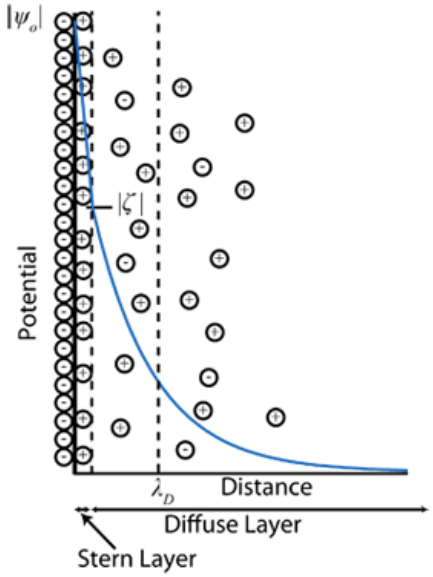

Figure 2: The electrical double layer where the potential ϕ is plotted in blue against the distance with in black a sketch of to how ions are distributed in such a potential. Denoted are the stern layer and diffuse layer and a few related variables resp. the zeta potential ζ to where the potential decays in the Stern layer and the Debye length λ_D the distance where the potential drops a factor $1/e$. Source[5].

2 Theory

In most of this theory chapter I will give introductions to physical phenomena related to optical scattering of small particles required in the rest of this thesis. I will try to only assume high-school level knowledge of physics. But I will not go into full derivations if I can avoid it, so for a better understanding of these topics please consult the references.

In the last subsection (section 2.8) I will explain our prediction on what we expect to see in our microscope. Here I will go into the derivation of how we expect light scattering of a nanoparticle in a liquid to behave optically when an electric potential is present. For this theory I want to test the following hypothesis: "We find intensity variations proportional to the applied potential that we can best explain due to the electric double layer."

2.1 Electrical double layer

An electrical double layer forms in a liquid when an object is submerged in it. The submerged object absorbs ions present in the liquid on its surface or has a charged surface itself. These ions then attract oppositely charged ions in a second layer around the object. This second layer of ions screens the bulk from the charge around the object and is influenced by both thermal motion and electric forces.

Important terms relating to the electrical double layer include the Debye length, the Stern layer and electric potential[4]. The latter describes the work needed to move a unit of charge between two certain places within the described volume. The electric potential inside a electrical double layer has two regions which behave in a distinct way, see figure 2. At the surface of the object the first layer of absorbed ions is located. Next is a volume which is called the Stern layer, wherein the potential decays almost linear because the ions in this region are saturated. After the Stern layer the potential goes to the equilibrium value exponentially, where every Debye length (λ_D) from the particle the strength of the electric potential decreases a magnitude $1/e$.

2.2 Polarizability

Polarizabilty is the relative tendency of a charge distribution to be distorted by an external electric field [6]. A charge distribution like for example the ions in the double layer around a submerged particle have a

preferred shape, but when put in an electric field the negative ions prefer to sit in the direction of positive field and the other way around. This new distribution of ions functions as an electric dipole and thus induce its own electric field, which is called an induced dipole moment. Figure 1 shows this in a perhaps oversimplified manner.

For an isotropic medium the induced dipole moment relative to the external electric field is defined as the polarizability. And this polarizability is constant for electric fields that do not change other properties of the environment. This can be described by the formula $\alpha = \mathbf{p}/\mathbf{E}$, for polarizability α, induced dipole $\mathbf{p}$ and electric field $\mathbf{E}$.

2.3 Refractive index of solutions

The refractive index of a solution depends on the type of solvent, the type of solute and the concentration of the solute. The relation best describing this effect is the Lorentz-Lorenz equation[7]:

$$\frac{n_{12}^2 - 1}{n_{12}^2 + 2} = \phi_1 \frac{n_1^2 - 1}{n_1^2 + 2} + \phi_2 \frac{n_2^2 - 1}{n_2^2 + 2} \tag{1}$$

Where n_i is the refractive index and ϕ_i the volume fraction of substance i.

The refractive index of the solution, n_{12}, is dependent on the volume fraction of the solute and this can vary locally, for example because of an electrical potential moving the solute ions.

A more general variant of the Lorentz-Lorenz equation also relates it to polarizability [8]:

$$\frac{n^2 - 1}{n^2 + 2} = \frac{4\pi}{3} N \alpha_m \tag{2}$$

Wherein N is the number of molecules per volume unit and α_m is the mean polarizability.

A less general, but quite accurate, equation describing the refractive index of solutions is the phenomenological relation between refractive index and salt concentration [9], as follows:

$$n_{saltwater} = n_{water} + K x_{salt} \tag{3}$$

Where refractive index n depends on ratio of number density of salt ions and water molecules x_{salt} with some constant K.

2.4 Rayleigh scattering

In our microscope we will have particles much smaller than the wavelength we use to look at them, so we have Rayleigh scattering. The Rayleigh formula[10] describes the intensity of the light scattered by particles smaller than the wavelength of the light. The formula is as follows:

$$I = I_0 \frac{1 + \cos^2\theta}{2R^2} \left(\frac{2\pi}{\lambda}\right)^4 \left(\frac{n^2 - 1}{n^2 + 2}\right)^2 \left(\frac{d}{2}\right)^6 \tag{4}$$

With I_0 the incident light, θ the scattering angle, R the distance to the particle, λ the wavelength, n the breaking index and d the particle size.

For particles in about the same order of size as the wavelength of light Mie scattering is used. But, since our particles will be at least an order of magnitude smaller than the wavelength used, Rayleigh scattering is a proper description in our setup.

With the theory up to now we have a path linking the electrical double layer to intensity, which we will explore to more detail in section 2.8.

2.5 Fourier transforms

A Fourier transform decomposes a function in the frequencies (with amplitudes) that build it. Or in other words it changes a function depending on time or space, $F(x)$, in a function depending on resp. frequency or k-space, $f(k)$. There are several ways to transform a function from one to the other, here is one[11]:

$$F(x) = \frac{1}{\sqrt{2\pi}} \int_{-\infty}^{\infty} f(k) \mathrm{e}^{ikx} \mathrm{dk} \quad , \quad f(k) = \frac{1}{\sqrt{2\pi}} \int_{-\infty}^{\infty} F(x) \mathrm{e}^{-ikx} \mathrm{dx} \tag{5}$$

When you use this on a sine function in time you would find a delta function centered at the frequency of the sine, but for even slightly different functions the resulting Fourier transform can be very complicated. It may seem like this introduces more complexity and with it problems, but a computer is very good at calculating a discrete version of the Fourier transform for any function in a limited domain. This computer calculated discrete Fourier transform uses an algorithm called the fast Fourier transform (FFT) and is a powerful tool for analyzing data.

A FFT can be used to efficiently filter high and/or low frequency components from a set of data. Alternate options to do so usually require fit functions which typically take more computing time.

2.6 Potential induced reactions

When talking about (chemical) reactions we are talking about the chemical transformations from a chemical substance to another. Most of the time this means a change in the chemical bonds between atoms. For example the bond between the oxygen and hydrogen atoms in water atoms being broken and binding to themselves, following an equation as $2\,H_2O \longleftrightarrow 2\,H_2 + O_2$.

Reactions almost always have a probability of occurring in both directions and only when enough time has passed the reaction reaches equilibrium, where the reaction happens as often in either way. Very often the timescale for equilibrium to be reached is quite fast, in the order of seconds or much less, and often the equilibrium is very one sided, where almost, or all, material ends up at one side of the equation describing the reaction.

There will always be an equilibrium in a closed system if enough time has passed to reach it, but when the boundary conditions of a closed system are changed the resulting equilibrium changes. In experimental setups these boundary conditions can be changed to achieve a certain result and these boundary conditions include: temperature, pressure, electrical potential, the contents of the system and more. We are interested in changing the electrical potential to induce reactions in this thesis.

When changing the electrical potential using electrodes in the sample and looking at the region close to the electrode, we expect to find chemical reactions like molecules splitting in ions and/or particles chemically bonding with the electrode surface [12].

2.7 Cyclic voltammetry

Cyclic voltammetry[13] is a technique to investigate reduction, oxidation and electron transfer initiated processes. It is, together with other voltammetry techniques, widely used in industry to sense atom and molecule species of interest.

During a cyclic voltammetry (CV) scan the potential over two electrodes in a sample is changed and the resulting current through the sample is measured. The result is then plotted as in figure 3.

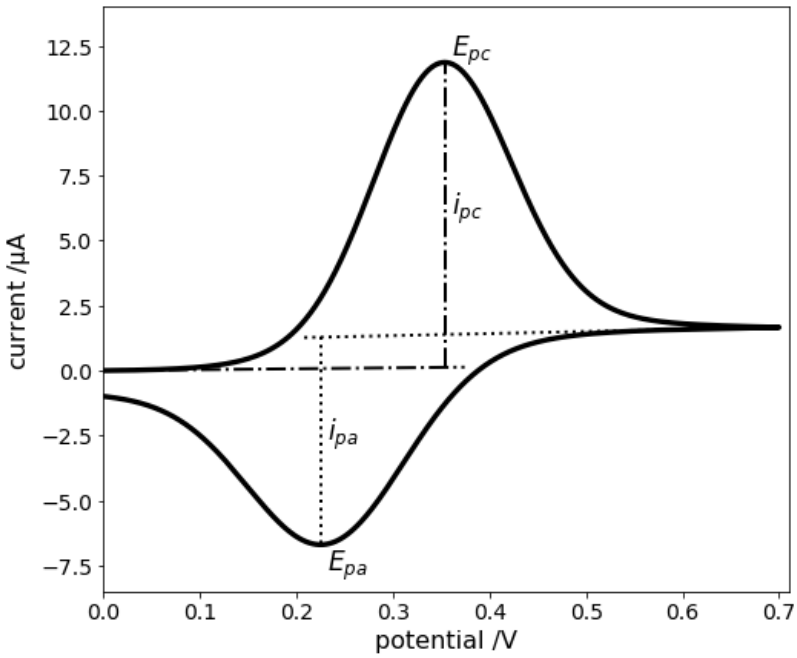

Figure 3: A CV scan from simulated data showing a common shape of such graphs. i_{pc} and i_{pa} are resp. the peak cathodic and anodic current and E_{pc} and E_{pa} the respective peak potentials.

Important parameters for a CV scan are the scan rate and the potential range. If the scan rate is very fast it is for example possible that a reaction hasn't fully equilibriated before the potential is reversed, which could for example result in the figure plotted to have no peak before reaching 0.4 volt.

Voltammetry is the category of measurements where information is obtained from the current running trough a sample due to a potential applied, CV is a subcategory of this where the potential applied is repeated instead of applied very slowly. We are mostly interested in cyclic voltammetry because we will measure many cycles which makes more sense to do for in our microscopy setup to reduce noise.

2.8 Prediction on potentiodynamic optical scattering

In this section I will derive our prediction for the potential dependent intensity variation based on the polarizability[14].

Working in the limit of relatively large surface potential $V \gg \frac{k_B T}{e}$ the ratio of polarizability due to EDL to the polarizability of the nanoparticle will give us insight to the relation between the intensity and the electrical double layer. With the wavelengths of the light used much larger than the EDL the charge distribution inside the EDL has negligible influence on the elastic light scattering. We derive a relation between intensity and the EDL by looking at a nanosphere with radius a in a regime where most screening is due to the Stern layer with screening ions uniformly distributed around with a thickness d, where $a \gg d$.

We have the number of excess ion charge in the screening layer given by $N = \frac{CV}{e}$ where C is the bulk capacitance, $C = 4\pi\epsilon\epsilon_0 a$, and e the elementary charge. We can rewrite this using the Bjerrum length $\lambda_B = \frac{e^2}{4\pi\epsilon\epsilon_0 k_B T}$ to:

$$N = \frac{a}{\lambda_B} \frac{Ve}{k_B T} \tag{6}$$

We can use the Rayleigh approximation to calculate the polarizability of a nanoparticle much smaller than the wavelength of the light. Because we are in the independent Rayleigh scattering regime the polarizability of the combined system of the nanoparticle and its electrical double layer is their sum. The Rayleigh polarizability in cgs-units[1] is defined as:

$$\alpha = 3V_{olume}\frac{m^2-1}{m^2+2} \tag{7}$$

For polarizability α with V_{olume} the volume of the particle and m the ratio between the refractive index of the object and its surrounding medium.

The polarizability of the surrounding solvent changes depending on the ion concentration. This can be described by the empirical relation $n_{EDL} = n_w + Kx_s$, where x_s is the ratio between the number density of salt ions and water molecules. Using this empirical relation in equation 7 and filling in N from equation 6 we find a final ratio between the polarizations α_P, the particle in a situation without potential, and α_{EDL}, the changes to the EDL due to the potential, as:

$$\frac{\alpha_{EDL}}{\alpha_P} = \frac{2K(m^2+2)}{n_w(m^2-1)} \cdot \frac{Ve/k_BT}{4\pi a^2 \lambda_B \rho_w} \tag{8}$$

Where ρ_w is the density of water molecules and $m = n_P/n_w$. Intensity next depends on polarization as:

$$I_{tot} \propto |E_P + E_{EDL}|^2 \propto \alpha_P^2 + \alpha_{EDL}^2 + 2\alpha_P\alpha_{EDL}\cos\theta \tag{9}$$

Where since $\alpha_P \gg \alpha_{ELD}$ and $\cos\theta \approx 1$ because there is no phase difference between α_P and α_{ELD} we get $\Delta I \propto 2\alpha_P\alpha_{EDL}$, where ΔI is the change to the light intensity based on changes to the EDL. Which if we use equation 8 gets us a proportionality which we initially want to test:

$$\Delta I = c(K, m, T, a, \lambda_B, \rho_w)\, V \tag{10}$$

So the variations in intensity should be proportional to the applied potential (V) with some constant (c) that depends amongst others on K which is a property of the ions.

A hypothesis I would dare to make based on this would be: "We find intensity variations proportional to the applied potential that we can best explain due to the electric double layer."

[1] The centimetre-gram-second system of units.

3 Microscopy

My project depends largely on having a very stable version of a dark field microscope. Therefor it makes sense to give an introduction to the microscopy and stability techniques used. In this section I will explain the working principles of both the microscopy setup and how we keep this setup stable.

3.1 Dark field microscopy

Dark field microscopy is, in a nutshell, looking at the diffused light by your sample while making sure the illuminating light beam isn't observed. In dark field microscopy your background is black, and your sample is bright. It is easier to explain using a figure, figure 4 shows a schematic setup of a dark field microscope. In figure 5 a dark field and bright field image of the same sample are shown.

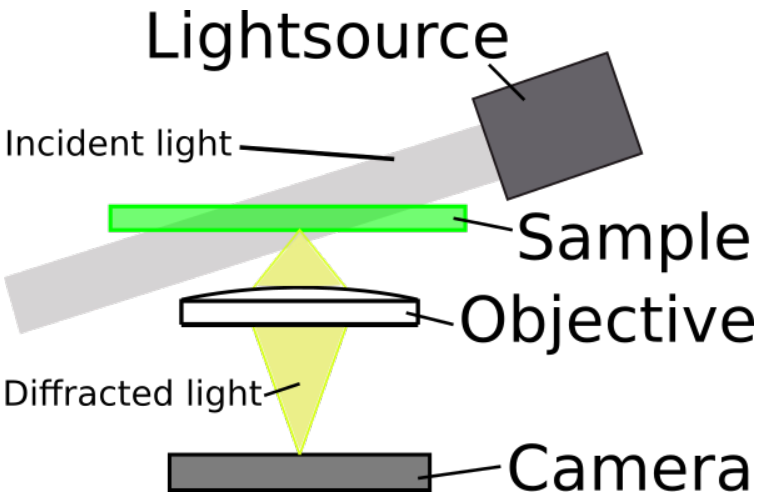

Figure 4: Schematic setup for a simple dark field microscope with camera. The incident light is scattered by the sample which is imaged by the objective while incident light is not reaching the the objective.

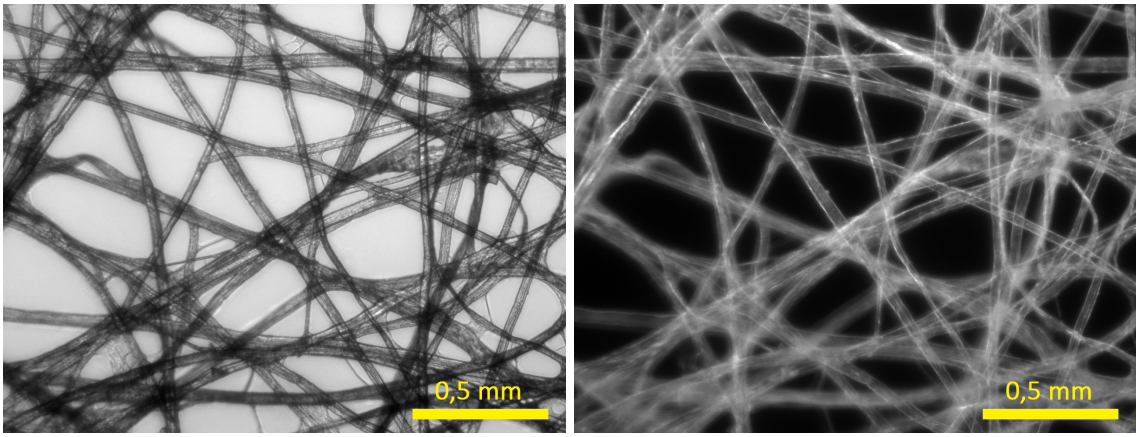

Figure 5: A bright field (left) and dark field (right) image of the same sample (a piece of tissue paper). Source of both images: Dark-field microscopy on Wikipedia.

3.2 Total internal reflection microscopy

Total internal reflection microscopy [15] (TIRM) illuminates the sample in an interesting way but is otherwise very similar to dark field microscopy, here I explain how it works. TIRM is in principle the same as dark field microscopy; the light used to illuminate the sample doesn't reach the camera. The difference is that the incident light doesn't directly reach the sample either, it totally reflects at the interface between the sample slide and the sample. This total reflection creates an evanescent wave[2] inside the sample region close to the interface. This evanescent wave then scatters of particles and the scattered light can then be seen trough the microscope. In figure 6 this is shown schematically.

Total internal reflection microscopy is a microscopy technique that I will be using because it has certain advantages over dark field microscopy. TIRM is useful because we are only interested in the region close to the interface and TRIM only illuminates in this region, up to a few hundred nanometers[16], of the sample because an evanescent wave decays exponentially. It is also beneficial to us that the reflected beam when using TIRM moves when the sample moves because we can use the changed position of the reflected beam to correct the focus of our microscope, see chapter 3.3 on PID loops.

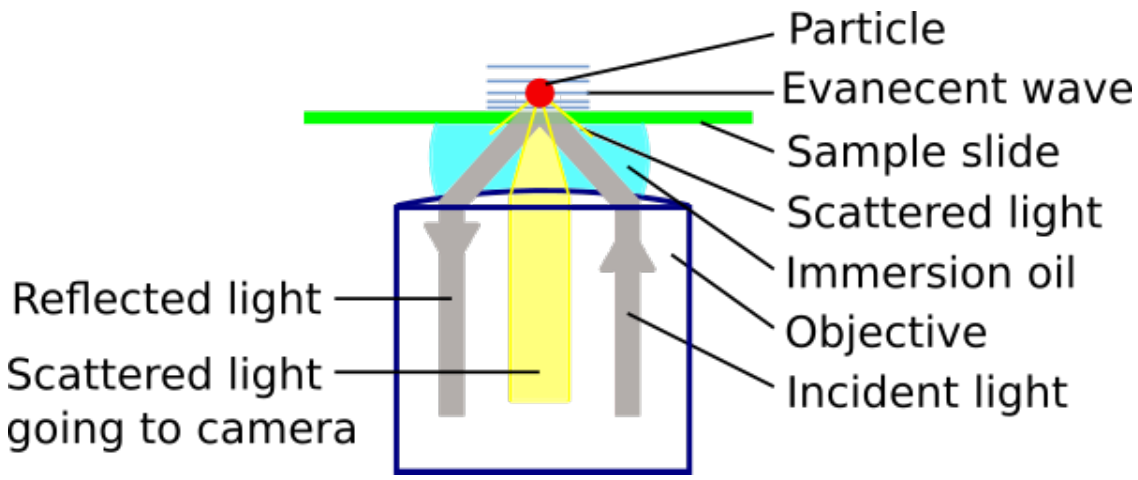

Figure 6: Schematic view of total internal reflection microscopy. The incident light is reflected by the edge between the sample slide and the solution of particles. This creates an evanescent wave in the solution which can scatter of particles.

3.3 PID controlled stability

A proportional–integral–derivative (PID) controller is used in our setup to keep the sample in focus. A PID controller continuously applies corrections to some input to keep a desired output[17]. It uses the difference between the desired output and the actual output, often called the error, to calculate a correction. This calculation has three parts that can be individually tuned using the parameters P, I and D for resp. proportional, integral and derivative of the error.

In our setup we have the reflected light from the sample slide that is related to the focus of our sample. If our sample drifts out of focus we see the reflected light move. Using the position of the reflected light when our sample is in focus as our base we can measure the error of the focus, which we can supply to the PID controller. The PID controller uses the drift of the reflected light to control the piëzo[3] in our setup which controls the sample position.

[2] An evanescent wave is an oscillating field that doesn't propagate.

[3] A piëzo, or piëzo electric actuator, is a machine holding a crystal that slightly changes shape when an electric field is applied. Often used to very accurately (up to a few nanometer) control positions in experimental setups.

4 Materials and methods

In section 3.2 I explained the working principles of total internal reflection microscopy and in this section I want to describe our specific setup and explain how we used it.

I will mostly go into details of why we have each part, not the exact distances of how the setup is lined out or how the code, that controls the setup, was written. More details are available in the appendix.

Our sample, section 4.7, is why this technique is possible. Its geometry and materials allow us to apply an electrical potential to the surface we totally internally reflect from in our TIRM setup. So it is very important for connecting the electronics, section 4.4, with the optics, section 4.2.

The last part, section 4.9, of this section describes how an actual measurement could be done. Here the usage of the UUTrack software, section 4.8, is assumed.

4.1 Experimental setup

Figure 7 shows the various parts of the setup in a very schematic way. The parts in this schematic will all be described in the rest of this section. There are some abbreviations used in the figure: Data AcQuisition system (DAQ), Quadrant Photo Diode (QPD) and Charge Coupled Device (CCD). The latter is the light sensitive part of certain cameras.

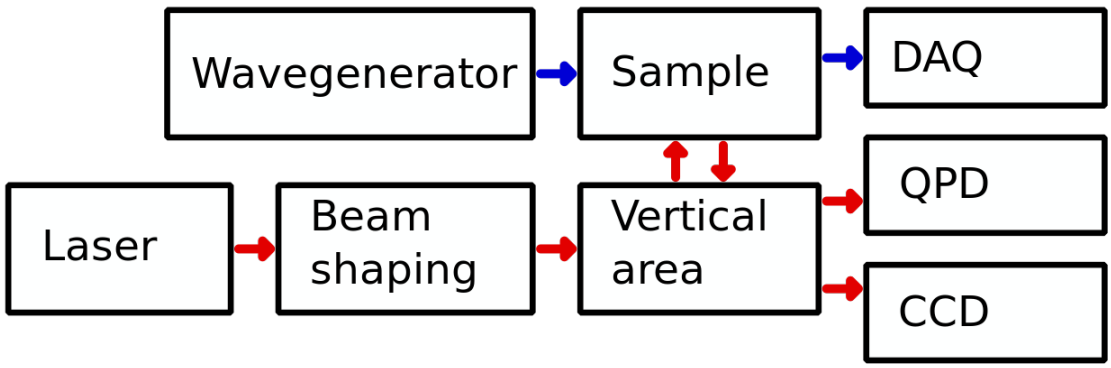

Figure 7: Very schematic view of the setup. The various parts are connected with arrows that are red when it is a light connection and blue if it is an electronic connection.

4.2 Optics

Before the light enters the vertical area we make sure it has the properties we want. We need laser light because total internal reflection microscopy needs a single wavelength of light to work best and we need illumination with high intensity to get enough signal. It is collimated and increased in size using two lenses on either side of a tube. This is necessary to illuminate enough area of the sample. Then a filter reduces the intensity when needed, this filter can be changed depending on the size of the sample particles. A polarization filter filters the light to a single polarization before the light enters the vertical area.

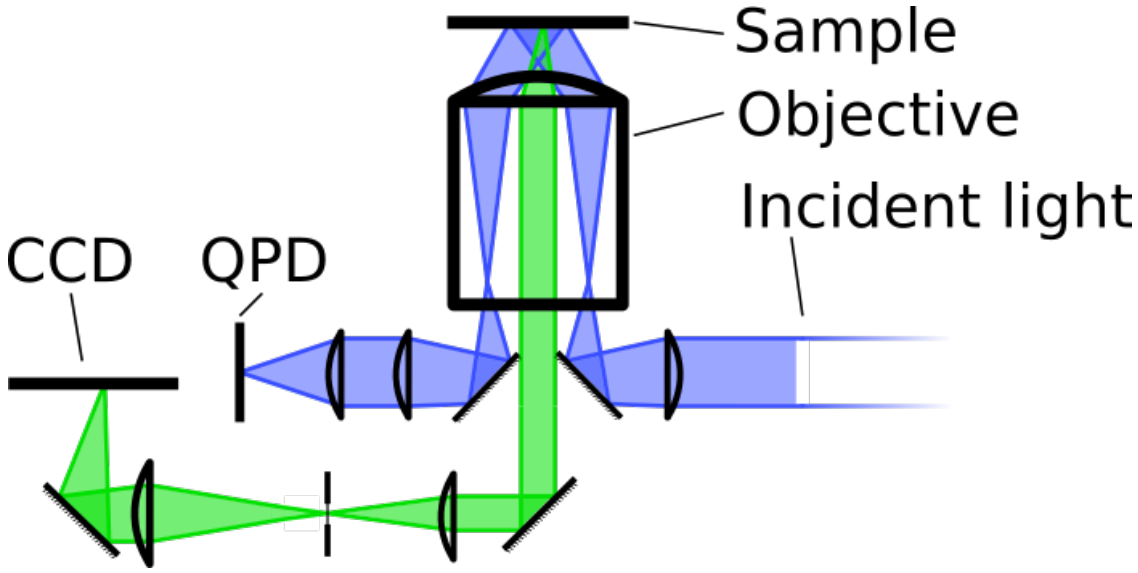

Figure 8: Schematic view of light path in the vertical part of the setup. Not annotated are the mirrors, lenses and a pinhole. The light path in blue is the light from the laser that after totally reflecting ends up at the QPD. The light path in green is the scattered light from particles in the sample that ends up at the CCD.

The main part of the vertical area, figure 8, is a set of two small mirrors in front of the objective that have a special role. Via one of the small mirrors the light is focused at one side of the rear focal plane by a lens. By entering from one side of the objective it reaches the sample under an angle large enough to totally reflect. The reflection travels back trough the same objective to come out on the other side of the rear focal plane. The other small mirror reflects the light trough another lens to make it collimated again. Between the two small mirrors there is a space where scattered light from the sample reaches. Irregularities and particles on the surface of the sample slide will scatter light that after traveling trough the objective and between the small mirrors goes towards our camera.

The two light beams exiting the vertical area are both used by the setup. The scattered light is focused on our camera by another lens. And the totally reflected laser light lands on a QPD after a filter reduces intensity to values acceptable by the QPD. The signal from the QPD is used to keep the camera in focus.

4.3 QPD controlled focus

A QPD has four areas that are sensitive to light and it outputs the difference in light intensity incident between the areas as a potential. The two outputs are the difference between the top two and bottom two and the left two and right two, so you know how far from the center a slightly focused light beam hitting the sensor is.

The signal from a QPD is used to correct the height of the sample stage. From figure 8 you can deduce that if the sample moves up, the light exiting the objective moves to the left and the light falling on the QPD moves down. This relation allows us to use the difference of the intensity on the top and bottom of the QPD to be the offset of the sample height and sent a corrected signal to the piëzo that controls the sample height.

4.4 Electronics

Applying a varying potential and measuring it at the same time takes quite a few connections between different apparatus. The circuit used to apply a potential to the sample is shown in figure 9. The potential is supplied by a wavegenerator that is connected to both the sample and a resistor. The DAQ is used to measure the voltage over each of the components.

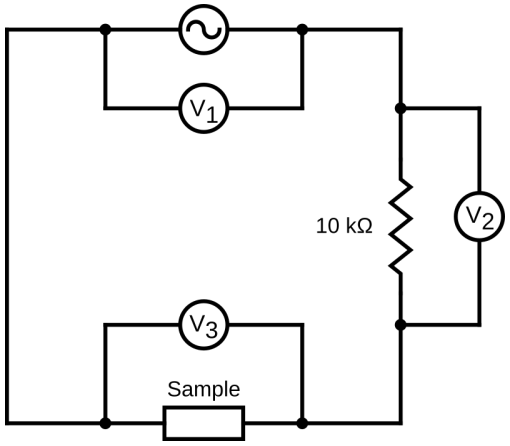

Figure 9: A schematic of the electric circuit around the sample. A wavegenerator supplies a wave over the sample and a high resistance resistor while the voltage is measured over all components. The voltages measured at V_1, V_2 and V_3 represent resp. the generated potential, the current and the applied potential.

When starting a measurement the DAQ is also used to blink an LED which is captured indirectly on the CCD. This flash enables us to synchronize the data from the DAQ and the movie.

The last electronic connection made is the trigger connection between the camera and the DAQ. To have data points from the DAQ that we can relate to the frames in the movie we use the trigger output from the camera as the clock for the DAQ measurements. This has the disadvantage of having less data points than possible from the electronic circuit in the setup. But when analysing we only need the points that correspond to the frames, so this method can be used to slightly reduce the work the computer needs to do.

4.5 Wave generation

For wave generation we have been using multiple sources: a programmed DAQ and a programmable wave generator from Agilent.

When we do not need a whole set of sequential different waves it is most convenient to use the programmable wave generator from Agilent because it is easier to use. The programmable wave generator is a box with buttons that can at any point in time be used to change the wave.

The programmed DAQ to be used as a wave generator is controlled by the microscope GUI, section 4.8. With it you can select a range of voltage offsets to cycle over and create a wave of the same amplitude and frequency for all of these offsets sequentially.

4.6 A transparent electrode

Indium tin oxide (ITO) is a compound of indium, tin and oxygen that has the property of being both conductive to electricity and transparent in the visible spectrum when in thin layers. These properties make it very useful for many things, for example in liquid crystal displays.

There are other materials like aluminium zinc oxide (AZO) that are also both conductive and transparent[18], but ITO is better suited for our needs. An advantage of ITO over AZO is that it is much more resistant to wear, which we need because we need it to be stable under relatively large potentials and in acidic conditions. The largest disadvantage of ITO is that it is more expensive than alternatives.

4.7 Sample

The sample is not very complex but very small and, because of that, hard to make. See figure 10 for a schematic image of our flowcell. Between the ITO (section 4.6) surfaces is a flow cell that we fill with solvent that we can change during an experiment. First we fill it with a solvent with particles and after some particles have landed in our view we change it to a solvent without particles. Then we can do measurements on those landed particles with the electrical potential between the ITO surfaces that we want.

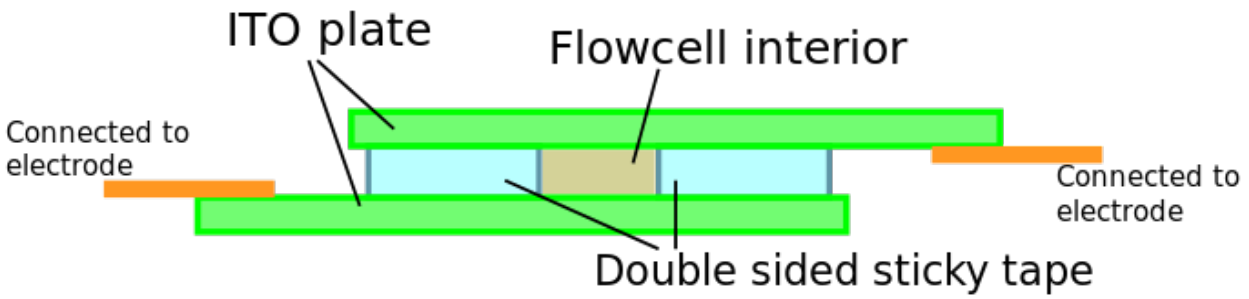

Figure 10: Schematic view of the sample slide. The double sided sticky tape doesn't conduct electricity and the ITO plates and connectors to electrodes conduct very well. The ITO coated slides act as electrodes for the solution in the flowcell interior.

A more realistic representation is shown in figure 11. In this image it is easier to see how the contents of the flowcell can be exchanged. When putting a drop of sample solution at one entrance to the flowcell capillary forces pull the liquid inside the flowcell. Any excess liquid can be removed with a tissue, where again capillary forces suck the liquid in. When the sample solution needs to be changed we can put a drop of the new liquid on one side and use a tissue to suck the liquid in the flowcell from the other side. This will replace most of the liquid inside the flowcell, but to ensure near complete replacement of the liquid inside we repeat this a few times.

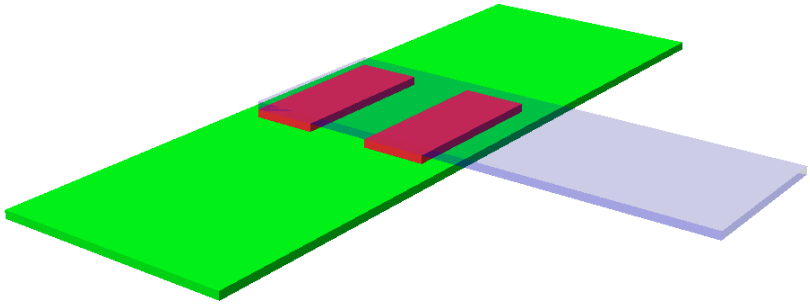

Figure 11: An isometric view of a 3D model of the sample slide, not exactly to scale. The ITO coated slide (green) and ITO coated plastic slide (opaque blue) are kept apart by two bits of double sided sticky tape (red) which creates a tunnel that we call a flowcell.

The flowcell works quite well for almost completely replacing the contents. We have used sample solutions with particles inside where after replacing the sample liquid no particles could be seen anymore. And while not measured directly, just by replacing the liquid many times the ions should be mostly replaced even if they mix fast enough.

Our flowcells usually have the following dimensions: $3mm$ wide, $6mm$ long and $0.4mm$ high, this gives them a volume of $7.2\mu l$. The height is determined by the double sided sticky tape but the other dimensions can be varied during the production. When filling the flowcell it is possible to leave a droplet around the entrance to increase the time before the sample dries. We usually use $20\mu l$ to fill the sample and leave the excess as a droplet.

4.8 UUTrack software

To efficiently use the microscope and get the most out of all the hardware used there was a lot of programming done. When I started my master thesis there was already a good microscope controlling software written called UUTrack. This software was great but more focused on particle tracking than imaging small variations. So a lot of additions to the original code have been done.

In appendix B I shortly explains all the files regarding UUTrack used for this project.

Additions to the code are various background correction modes for the live display in the GUI (guided user interface), a widget which displays some information from the image like the amount of over saturated pixels and the integration of all the uses of a DAQ.

The various background corrections modes are useful for identifying when it is worth it to save the data. It is especially helpful for recognizing if particles land when their signal is similar to the background variations. And it also helps to see intensity variation due to the applied potential while measuring, this is possible when the variation is very big.

The added widget is a popup screen which displays many things that can be interesting while using the microscope. The amount of over saturated pixels is useful because you do not want these pixels with unchanging signal since we are interested in the intensity variation. Another thing it shows is the variation in the current frame, this should be high when the image is in the correct focus. It also shows a plot of the absolute change to pixel intensity per frame, this kind of plot can give useful information on the stability of the setup.

The DAQ is used to do many tasks: acquisition of potential data, wave generation and to flash a LED, which makes it possible to synchronise while analysing the data. Whenever you chose to record a movie with the camera the DAQ will automatically be used to save the data on the potential and it will flash a LED which is aimed on a spatial filter in the path towards the camera, this always causes a clear spike in intensity on the camera image and we can use it to synchronise the two otherwise separate data sets. To generate a wave or set of waves using the DAQ from the UUTrack software is more useful when generating a set of waves because a out of the box wave generator is slightly easier to use.

4.9 Method

I will describe the steps to do a simple measurement while going into a little bit of detail.

A while before starting a measurement it is necessary to start the laser so it can heat up before the measurement, an hour seems a good estimate. Until the sample is correctly in place keep the laser blocked to avoid eye damage. While waiting for this it is quite possible to create the flowcell(s) for that day's measurement and have a long coffee break.

Preparing the microscope First put the sample (section 4.7) in the sample holder. To do so the objective must be cleaned with for example iso-propanol and a tissue to get rid of leftover immersion oil. Then add new immersion oil and gently drop the sample in place, trying not to move it vertically too much to avoid dragging oil between the sample and the sample holder. Then place the magnets that hold the sample down and connect the electrodes, try not to obstruct access to the flowcell with these electrode connections.

With the sample in place the GUI can be started to get an image. The flowcell can be filled with a solution that makes sense for your experiment, probably a solution without particles is best to start with. Fill the flowcell using a pipette: put a drop, about $20\mu l$, on one side and it should go all the way through the sample. Turn on the camera, possibly change a configuration file and then start the GUI. Use the GUI to start previewing the camera image, you will not see anything since you are not in focus yet.

Focusing the camera When focusing the image the piëzo stage must be used. Use the piëzo controller program (APT controller) to start the piëzo and put it at approximately 30 volt, about the middle of the range of the piëzo.

If the setup was in a similar focus last time it was used it is possible to skip some steps and immediately start the focus loop to find the focus. Then you can immediately look for a nice area to measure.

Otherwise use the manual focus knob to find the focus. The focus can be recognized by inevitable speckles of dust still on the sample slide that should appear as as sharply edged dots as possible, usually in a slightly horizontally elongated shape due to the polarization of the illumination. To ensure you are in the focus you can use the vertical translation knobs to move the sample; if the dots you see move as you do they are from the sample.

When in focus use the knob to angle the reflected light coming out of the objective towards the QPD on the center of the QPD. This position is visible from the signal on the piëzo controller software, in the large corsair there should be one small circle moving when adjusting this. The small circle should be in the center horizontally.

When the reflected light to the QPD is also aligned start the focus loop. For the focus loop to work there should be enough but not too much signal hitting the QPD, this might require adding or removing a filter in front of it. The amount of signal on the QPD is shown in the APT controller software as a vertical bar on the right that should not be zero or maximal.

Then focus the image from the camera again using the knob to angle the reflected light, which results in a new focus because of the focus loop is now changing the voltage to the piëzo. Keep in mind that the charge

to the piëzo shouldn't get close to 0 or 75, the minimum and maximum of the piëzo, while in focus loop you can use the manual focus knob to mitigate this without changing the actual focus.

Now you can look for a nice area of the sample to do your measurement using the translation knobs on the setup. Possible nice features include typical ITO regions and very dust speckle free areas.

Preparing directly before the measurement Most mechanical adjusting is now over and this is a good time to change the settings of the GUI. Settings to change are the binning, the range of interest (ROI) and the name of the movie when saved.

The last step before pressing continuous saves is to put the desired potential over the sample using a signal generator. With the potential between -2.5 and 2.5 volt you are probably safe from irreversible changes to the sample. However this is just an estimated from experience, new experiments can change our understanding of this drastically in all directions.

When using the DAQ as wavegenerator from UUTrack you also need to change these settings in UUTrack and remember to start the generation when measuring.

When saving data it is possible to measure indefinitely by binning 2 by 2 and running at 200 FPS in a slightly smaller region but try not to make files over 20 Gigabytes because if they corrupt you lose so much data.

Closing the setup When done with measuring everything can be turned off except the piëzo controller program which is best left deactivated but running because it usually saves the focus. So put the piëzo in open loop and deactivated.

It is best to take the sample out and clean the objective as well. This is especially necessary when it otherwise would be in the setup for more than a few days before being removed. Putting a slide over the objective without oil can be useful for protecting it from dust.

5 Calibration

Before I use the setup I first want to know what it is capable of. To find out more about the capabilities of the setup I have done some experiments that are described in this section.

First I calibrate the magnification of the microscope, section 5.1, and then I work on identifying particles in the image, section 5.2.

Because we need a very stable setup the drift was also subject to many experiments. This is described in section 5.3 and 5.4, respectively on long and short term drift.

5.1 Magnification of setup

To measure the magnification we use a calibration slide with 10 μm dividers and calculate the distance it images on the cameras pixels. From the documentation of the camera [19] we know that each pixels spans an area of 6.5x6.5 μm^2.

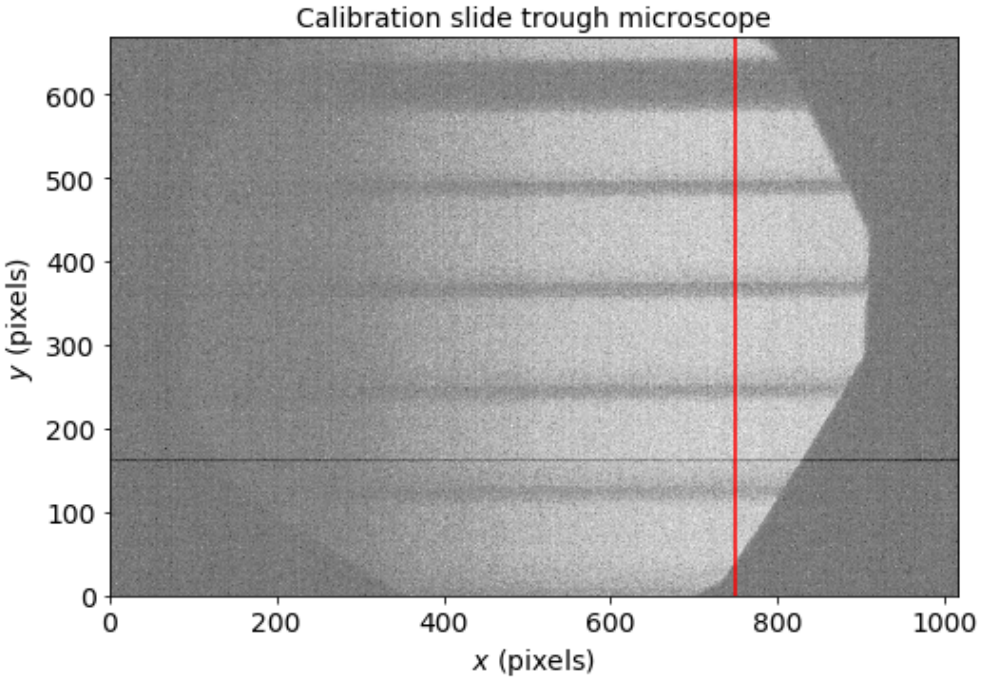

Figure 12: Image of calibration slide with 10 μm dividers taken with bright field imaging. The red line is the line chosen to calculate the magnification over. Note that this figure is binned 2x2, this also accounts for the horizontal line [19] around y=160.

I found a magnification of 157$\pm$3 times from calculating the distance in pixels between the furthest horizontal lines of the sample slide. Later measurements on material deposited in a grid of known separation confirmed this.

5.2 Identifying particles

A clean sample slide always still has some speckles from imperfections on it, but we have to recognize the particles we are interested in. When using ITO coated slides we can see a lot of these imperfections on it,

see figure 13.

Figure 13 shows a parallelogram shaped region and a line aligned with it to the left with relatively equal intensity speckles. This does not look like contamination from dust or dirt, which is usually in irregular patterns and of higher intensity when we do see it. We refer to these individual ITO speckles in a regular pattern as grains.

Figure 13: When imaging a clean slide of ITO there are many features visible. The trapezoid region of speckles/grains resembles the roughness of the ITO surface when imaged using AFM, figure 14.

We compare our images to other images of ITO slides and had the possibility to look at one of our slides under an atomic force microscope (AFM). From these other sources we confirmed that there were in fact rough regions of ITO grains in parallelogram shapes present in the ITO, see figure 14.

We think these regions are created by the releasing of stress in the ITO layer in the annealing process in the creation of the slides[20].

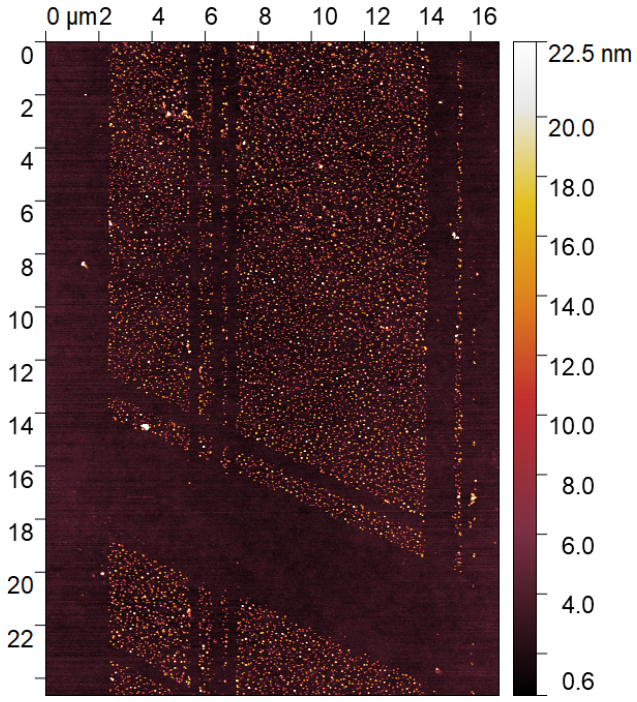

Figure 14: An ITO slide under an AFM. We guess the rough trapezoid region is a region of regularly spaced "grains" of protruding ITO material caused by the creation process of these ITO slides.

To introduce particles we replace the solution within the flowcell with a colloidal solution of the particles we want to study. Usually the particles do not tend to land very often. This is probably due to our particles, usually made of gold or platinum or titanium, and our slides being negatively charged, making them repel each other. However when they do land they stay landed even when we change the solution in the flowcell back to a solution without colloids. We can monitor this whole process trough the microscope so we know what features in the image form the slide surface are particles coming from the introduced colloids.

Currently we are not able to distinguish based on intensity alone how large particles are. We can clearly see particles larger than $20nm$ and smaller particles are possible to see when using background corrections, see section 5.2.2. The intensity of particles should scale approximately squared by their volume, that is with the sixth power of diameter of spherical particles. We however haven't been able to, with certainty, find dimers (double particles) which would help us find out more about intensity scaling in our microscope.

5.2.1 Getting particles to land

It proved quite difficult to land negatively charged particles on the surface of a negatively charged slide. Most materials have an effectively negative charge when submerged in water and since same charged things repel each other this causes problems when trying to land a particle on a surface. To make this repelling force easier to overcome we can try to change the charge of the surface so it is actually positive and thus attractive. There is a known technique [21] for doing this using an enzyme called Poly-l-lysine. Using this enzyme we are able to land particles fairly consistently.

We have experimented with techniques for coating slides with Poly-l-lysine (PLL). We have had the most success by sandwiching two cleaned slides with PLL solution in between, to keep it from evaporating, and after about 5 minutes drying them with an air blow gun. Other ways that we tried are adding PLL directly to the sample when we want them to land and baking slides in an oven with PLL involved. This latter method did not work for us and the former method of adding PLL directly worked to some degree but it does potentially induce new problems with the extra particles in the sample solution.

5.2.2 Identifying particle landings

When tying to image small particles it is necessary to be able to distinguish them from the background. The microscope we have is very stable but the background is still quite noisy. This noisy background is stable in time, so we can make reasonable background corrections. Doing background corrections is possible using the GUI, section 4.8, but for really small particles this can be done quite well in data analysis.

To see how well this could be done I have made data of 20 nm sized gold particles. The data consisted of a glass slide coated with PLL with a gasket where a sample of 20 nm gold particles diluted 20 times with DI water. The particles would occasionally collide with the sample wall where they would stick. This was visible by eye, but to gain more accurate knowledge about the particles I analysed this using python.

To find landing particles in analysis I looked for the properties of a landing particle in the image. A landing particle will, after landing, stay in one place and have a constant intensity. We can make a background corrected image sequence where we take the last 5 frames as the background for the next one. This way when a particle lands it can be seen to regularly decay over 5 frames and any existing particles are not visible. The shape of this decay can be seen in figure 15(a) where the found particle decays are plotted.

Using the python package trackpy[22] we could analyse the background corrected image sequence and find landing particles. With trackpy we can find speckles in every image in the sequence within a assignable size and intensity range, where we look close to the expected values. Next we can use the same software to link the same speckles between different frames when they are close enough in distance and in time frame so they are probably the same speckle. Then we can look for speckles that decay as expected and plot their intensity before decaying, this can be seen in figure 15(b). The locations of these landings are shown in figure 16.

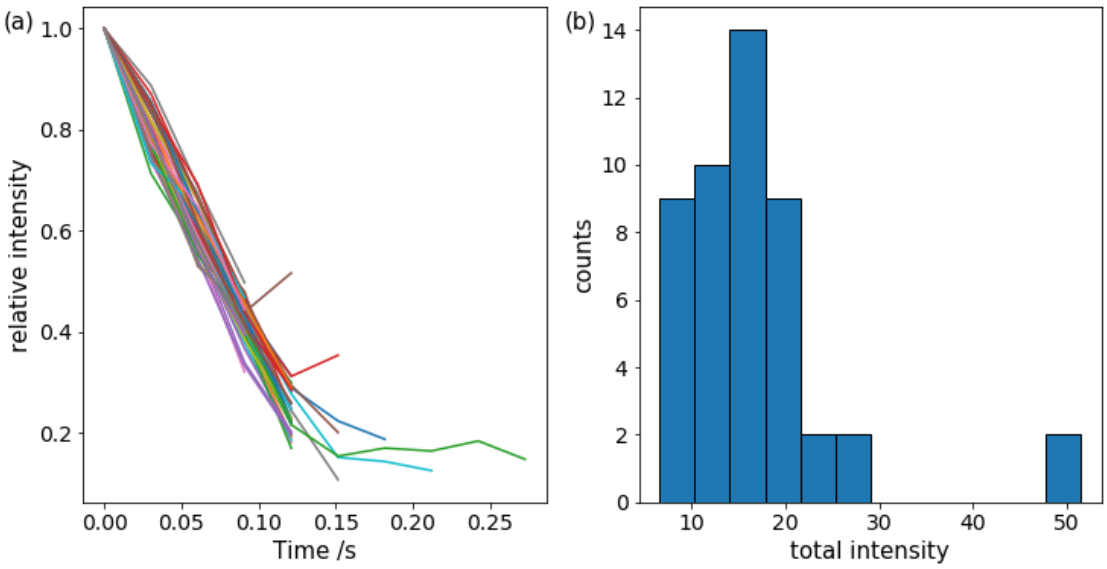

Figure 15: The (a) relative intensity in time and (b) histogram of the total intensity of the particles found landing.

In figure 15 there are a few peculiar features. In (a) the relative intensity for some landing particles did not decay completely as expected, for example by staying visible for longer or having increased intensity for a short time. This can be explained by instability of the setup or perhaps the particle shifting in position a little bit after a short time. In (b) the amount of counts is not particularly high, but with the strictness used when analysing this was to be expected. Also in (b) there are two counts at more than double the average total intensity, these particles might have been dimers.

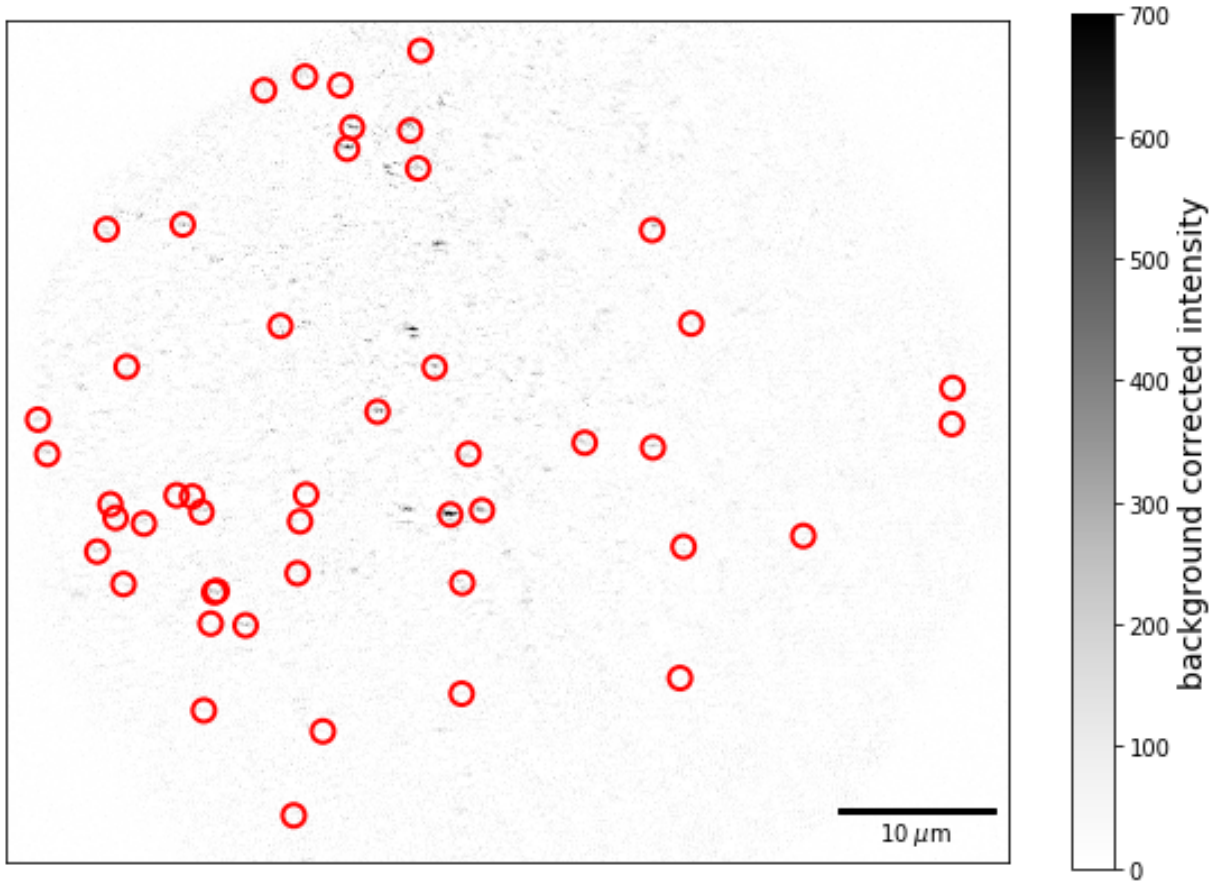

Figure 16: Background corrected image with the locations of the found landings encircled in red. The background used is the image before any landings and the subject to this background correction is the image after all the landings.

5.3 Long term drift

Every part of the setup is fastened as tight as possible to increase stability with the exception of the sample itself because it needs to be moved into focus. This exception is the source of a rather large amount of drift mostly perpendicular to the focus. This drift has a large amplitude in relatively long timescales, see figure 17. A change in intensity of a factor 1.3 is seen after 100 seconds for an uncorrected sample.

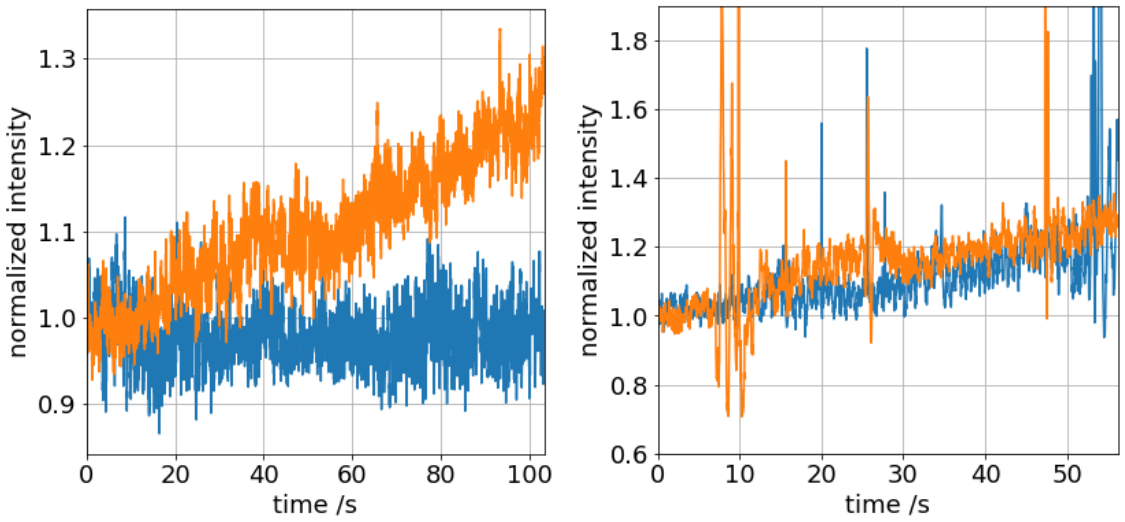

Figure 17: The normalized intensity with (blue) and without (orange) focus loop for the intensity of a sum of pixels in the camera image, normal noise on left and with artificial noise on right. Normal noise is while actively trying not to touch the setup and artificial noise made by leaning on optic table and tapping the setup stage. Without focus loop the intensity varies significantly more on long timescales.

To combat the large drift in long timescales we installed a PID controlled stability loop (chapter 3.3) based on the feedback from the reflected light from the sample on landing on a QPD (figure 8). With this in place the drift in long timescales is almost eliminated, see figure 17. The normal noise case has almost no change in normalized intensity after 100 seconds when using the PID loop. When making artificial noise there is a change in intensity even when using the PID loop, this could be from the sample moving in the horizontal plane which is not corrected for and can easily happen when being rough with the setup.

5.4 Short term drift

We also have short term drift in our sample, where I take shot noise to be part of the short term drift for simplicity. We cannot get all of this drift away, but plan to have it under control such that we can still see our signal.

This happens in all directions and some if it can be avoided by careful use of the setup. For instance someone walking by the setup will shake it left-right, up-down and out of focus. However, this shaking and other short term drift like shot noise can be averaged out over time since they don't change the mean of a long time measurement.

Using the PID we can introduce more short term drift, see figure 18.

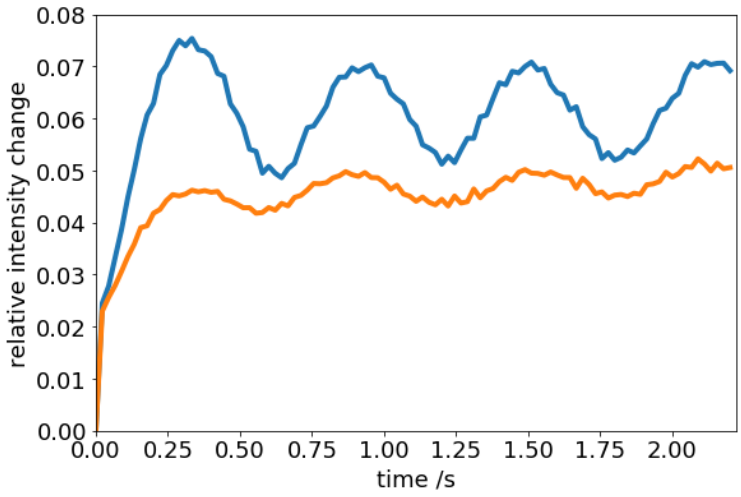

Figure 18: With (blue) and without (orange) PID loop the short term average intensity variation.

The short term drift is worse when using the PID loop, possibly because its corrections cause constant small changes. There also seems to be a periodicity of about 2 Hz in both measurements that is more pronounced in the measurement with the PID loop working. This periodicity is probably due to some external source and is still seen in the average because of normalization, when normalized on a low value the resulting variation is relatively larger. This periodicity could be a problem when measuring at the exact same frequency, however we often measure the same sample at multiple frequencies so this should never be a problem.

It is possible that with better settings for the PID loop we can reduce the short term drift, or at least reduce the increase in short term drift due to using the PID loop.

6 Data processing

Without data processing the raw data we collect we cannot use it to its full extent, but we need to take care not to distort the results. This section explains how the various steps in data processing should work and argues why we make various choices.

Section 6.5 explains why we chose certain representations for the data. These representations are then used in the results, section 7.

More information on the actual files is in appendix C.

6.1 Particle selection

In our movies there are usually less then ten particles so we do not think it is worth the effort to automate choosing particles, we will manually check for mistakes of such an automated system anyway. We manually select each particle, assisted by some code to find the peak intensity, and sum over the nine pixels around and including the peak. Other ways of finding and selecting an area are also possible.

We will create intensity versus time and/or intensity versus applied electric potential plots for all of the selected particles. The intensity variation varies in many ways of which examples how to distinguish between them are whether they correlate or anti-correlate with the applied potential or whether they are linear or curved between the peaks. After processing the particles we find the usual behaviour of the particles by looking how the majority acts.

6.2 Drift correction

With the focus lock we take care of most of the drift, but some of the drift has different causes and needs to be taken out in data processing.

To take out drift in data processing we can either use Fourier transforms to create a fit for drift correction or fit a polynomial. Because we do not want to correct for effects due to the applied potential we use low order fits.

The fits shown in figure 19 can both work as drift corrections but have different advantages. The polynomial fit is very smooth and follows the drift in the sample well without leaving large artifacts at the edges. It however does not correct for the small and sudden drop around 180 seconds. The fit from Fourier transforming has some artifacts at the edges and varies around the polynomial fit slightly. It does however also provide a correction for the sudden drop in intensity around 180 seconds.

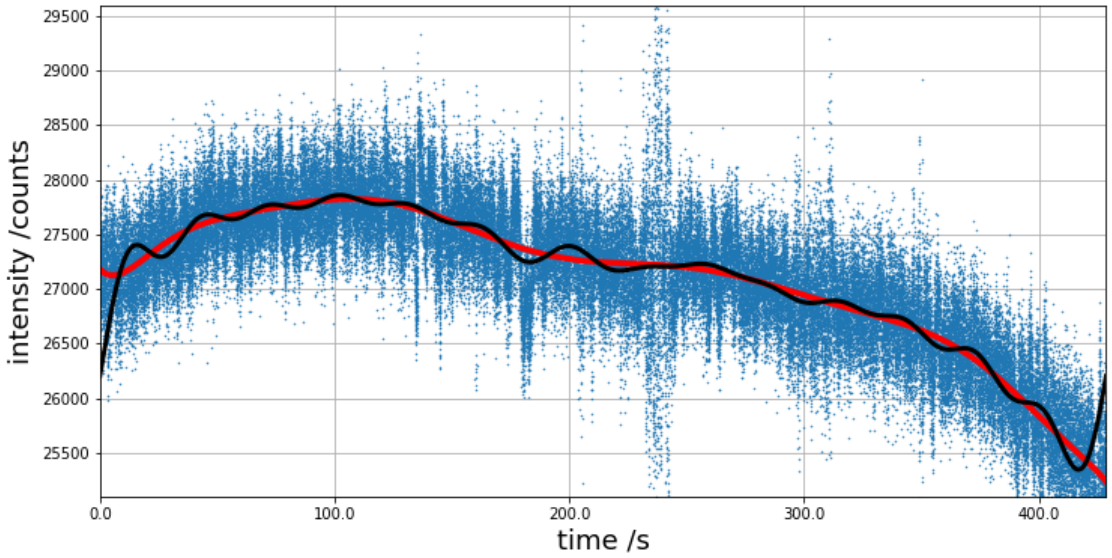

Figure 19: Intensity in time (blue dots) for 1.5 V amplitude 0.2 Hz frequency measurement on Platinum particles in pH 7 phosphate buffer, 12th order polynomial fit (red line) and up to 16th order Fourier transform (black line).

We use Fourier transforms instead of a fitted polynomial because we found it more consistent and less calculation intensive. While the Fourier transform does often have artifacts at the edges, these edges are often part of not complete cycles that we do not look at either way. There is also no chance of introducing features with the frequency of the potential because the Fourier transform can be specifically chosen not to do anything at that frequency.

6.3 Cycle averaging

To gain a clear enough signal within one cycle of potential variation we need to average over many cycles.

We have looked at various methods for finding cycles and have eventually found one that works consistently. Our current best method finds the period and offset of the applied potential as good as possible and uses this to find the start of cycles from where it averages over all the full cycles in the data.

Finding the period and offset of the applied potential are what we have struggled with most. Currently we first approximate the period by taking a Fourier transform and then try to find the peak values of the applied potential at approximately that interval. This gives us a list of array index locations of the peaks in the applied potential. We take the average distance between them as the periodicity of the signal. The offset we find by taking the average distance left over from every peak to the start after reducing as many periods as possible.

The found period and offset of the applied potential can be translated to those of the movie. We know the difference in offset because of the overlapped peaks due to the flash of the LED, see section 4.4, at the start of the measurement. This clear peak in intensity in the movie can be aligned with the signal to the LED that is saved at the same time as the applied potential. And because all the data from the DAQ is recorded only when the camera takes a frame, the period of the applied potential and movie is the same.

Because the period and offset are not integers this requires some rounding off to use array indices correctly. We always round down which results in that we often have one ”missing” data point near the end of the

cycle. Otherwise this rounding of doesn't have much effect since we round both the potential and intensity down they have the same little offset, half a frame, from where the start should be.

To do the averaging we take the values from each successive period and average per frame in the period. Half periods at the start and end are simply left out.

6.4 Filtering anomalies

We have now corrected for drift between different cycles but we still need to filter cycles where there was a spike in intensity due to for example drift or a particle floating by or the setup being disturbed by humans.

We can look at every cycle individually, see section 6.3, and filter out the cycles with unexpectedly large intensity variations. We decided that a cycle is bad if more than 20 percent of the points in the cycle lie outside of 2σ of the mean value of the measurement, where σ is the variance of the full measurement. When this happens there are double the amount of points in this range compared to what is expected. This happens mostly when there an event where a sudden large peak in intensity followed by a few vibrations. We see such events are caused by floating particles or shaking of the whole movie, possibly due to human interference, and agree with the decisions made by the program to remove these points.

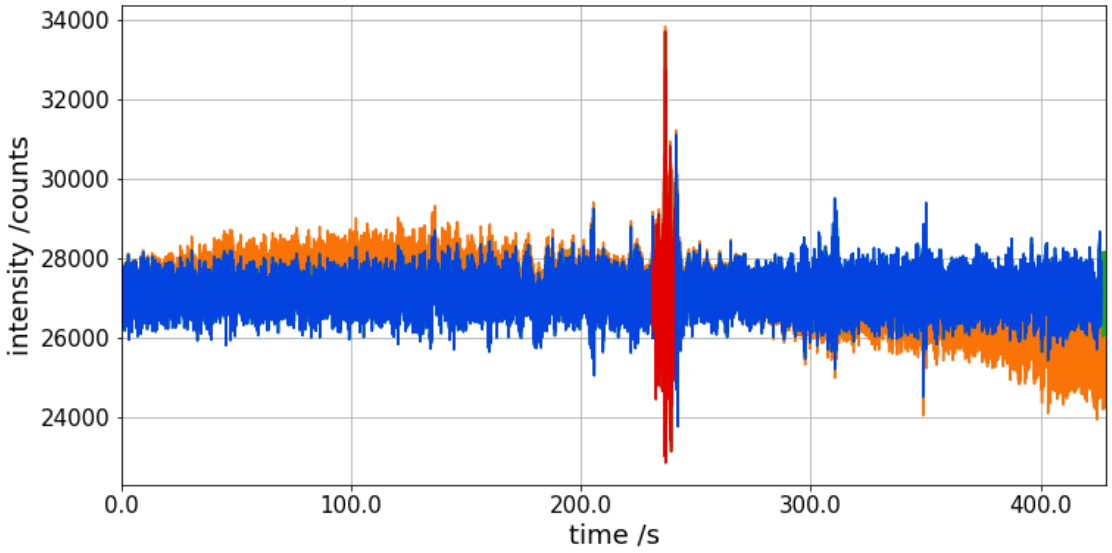

Figure 20: Anomalies filtered when more than 20 percent of points are outside of the 2σ range of the measurement. In orange the data before drift correction, in red the cycles that are filtered, in blue the accepted cycles and in green the incomplete cycles after correction. The data shown is from a measurement on platinum particles in pH 7 phosphate buffer.

In figure 20 there is one cycle rejected. It is rejected because more then 20 percent of its points are outside of the 2σ range of the measurement. If I had to chose myself I would say this cycles is the worst one of the measurement, so I think this automatic system works.

6.5 Possible graphs

After all this processing we have a lot of data that needs to be visualized in a good way. We have found the following styles the best final figures. The averaged potential and averaged normalized intensity versus time

in one plot is shown in figure 21. The averaged normalized intensity versus averaged potential is shown in figure 22.

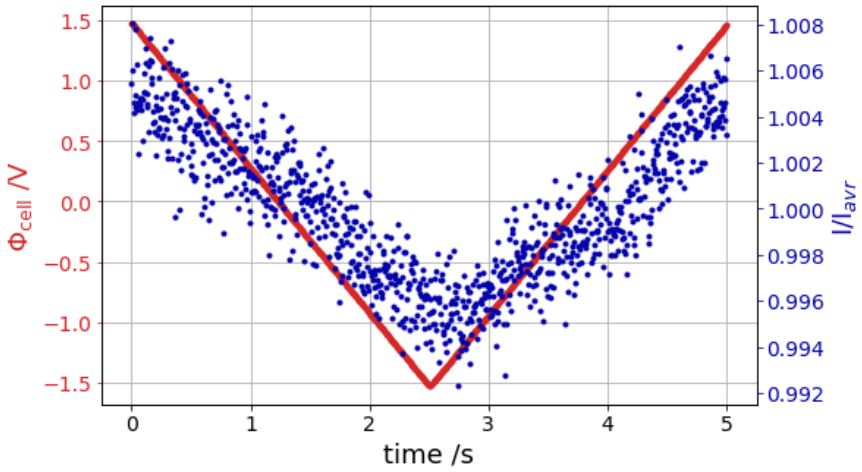

Figure 21: The averaged potential (red) and averaged normalized intensity (blue) for one period.

We can report most of what we are interested in from these two types of figures. Figure 21 is useful because it makes the timescale and phase difference between the potential and normalized intensity clear. Figure 22 is useful because it clearly shows the proportional relation between the applied potential and normalized intensity. Also any features present around a certain potential become more clear.

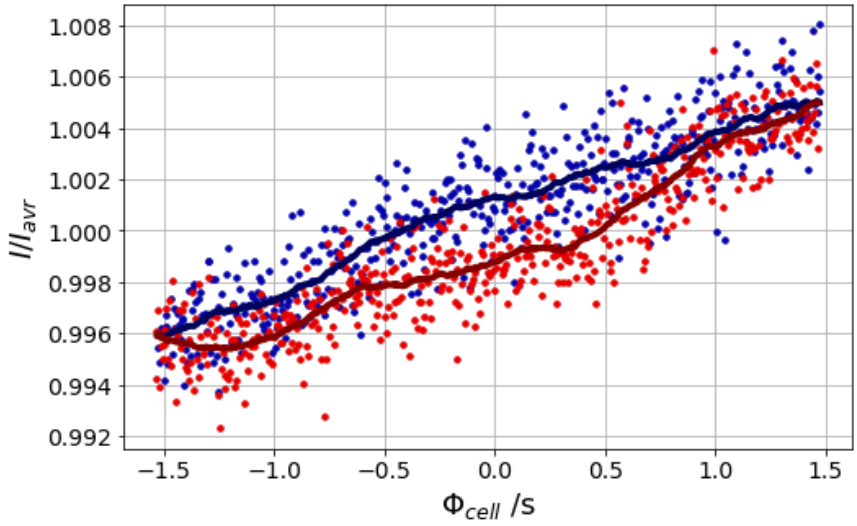

Figure 22: The averaged normalized intensity versus the averaged applied potential. Dots for the individual points in the cycle and lines for the smoothed curve trough the points, with rising potential is in red and dropping potential in blue.

7 Results

Since the technique of looking at intensity variations depending on changes in polarizability caused by an electrical potential is new I will first provide results to support this.

Next I will provide results of two other experiments. One will focus on a different sample; a sample where Chromium particles where deposited. And the other will focus on applying potential in a different way; a potential with variable offset.

7.1 Intensity change proportional to polarizability

I predicted a proportionality between applied potential and intensity based on the electrical double layer. Measuring the proportionality would not be enough to prove this prediction, but that is great first step. I will therefor first present experiments to support this. To address the claim this is caused by the EDL I will show evidence both from the temporal behavior and the scaling depending on ion optical polarizability as discussed in chapter 2.8.

Already in early experiments we see the proportionality between potential and intensity, along with other effects we can now explain. Figure 23 shows the first results clearly displaying the linear behavior of the intensity depending on applied potential. The measurement with higher potential range shows some nonlinear behavior we can explain with the high applied voltage inducing reactions in the liquid.

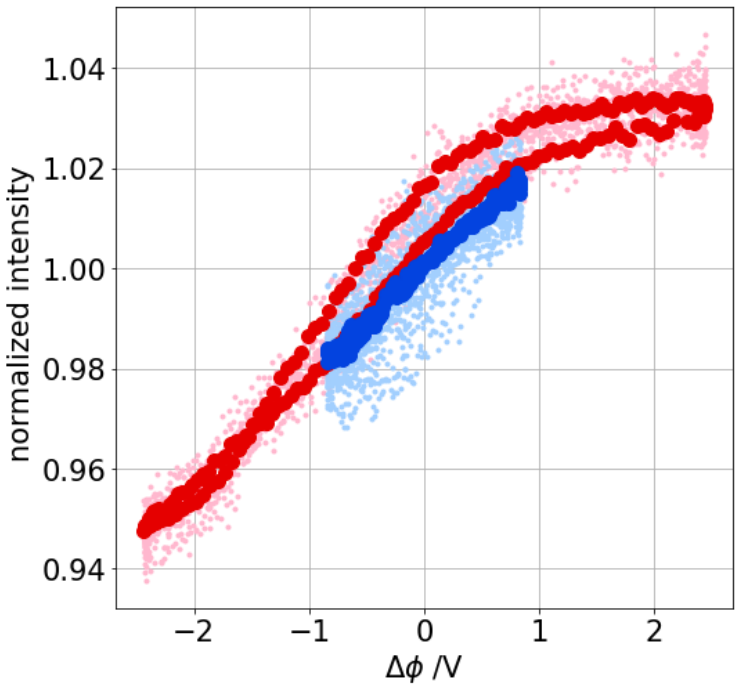

Figure 23: The normalized intensity change plotted as a function of the cell potential for ± 80 cycles (light symbols) and the average of all cycles after correction for drift (bold symbols) for two different sweeping amplitudes all at 1 Hz. The sample was an ITO grain in a phosphate buffer at pH 7.

We are now aware that these applied voltages are high enough to start chemical processes that are not negligible in the sample. For example the splitting of water into hydrogen and oxygen ideally starts at a

potential of 1.23 V. We however did not see anything extraordinary happen while measuring, like bubbles forming or the ITO surface changing. Our prediction on what optical effects we would see because of the EDL does also not depend on such reactions and shouldn't change as long as these effects are relatively small. Therefor we think our measurements can still be used for showing the proportionality between potential and intensity.

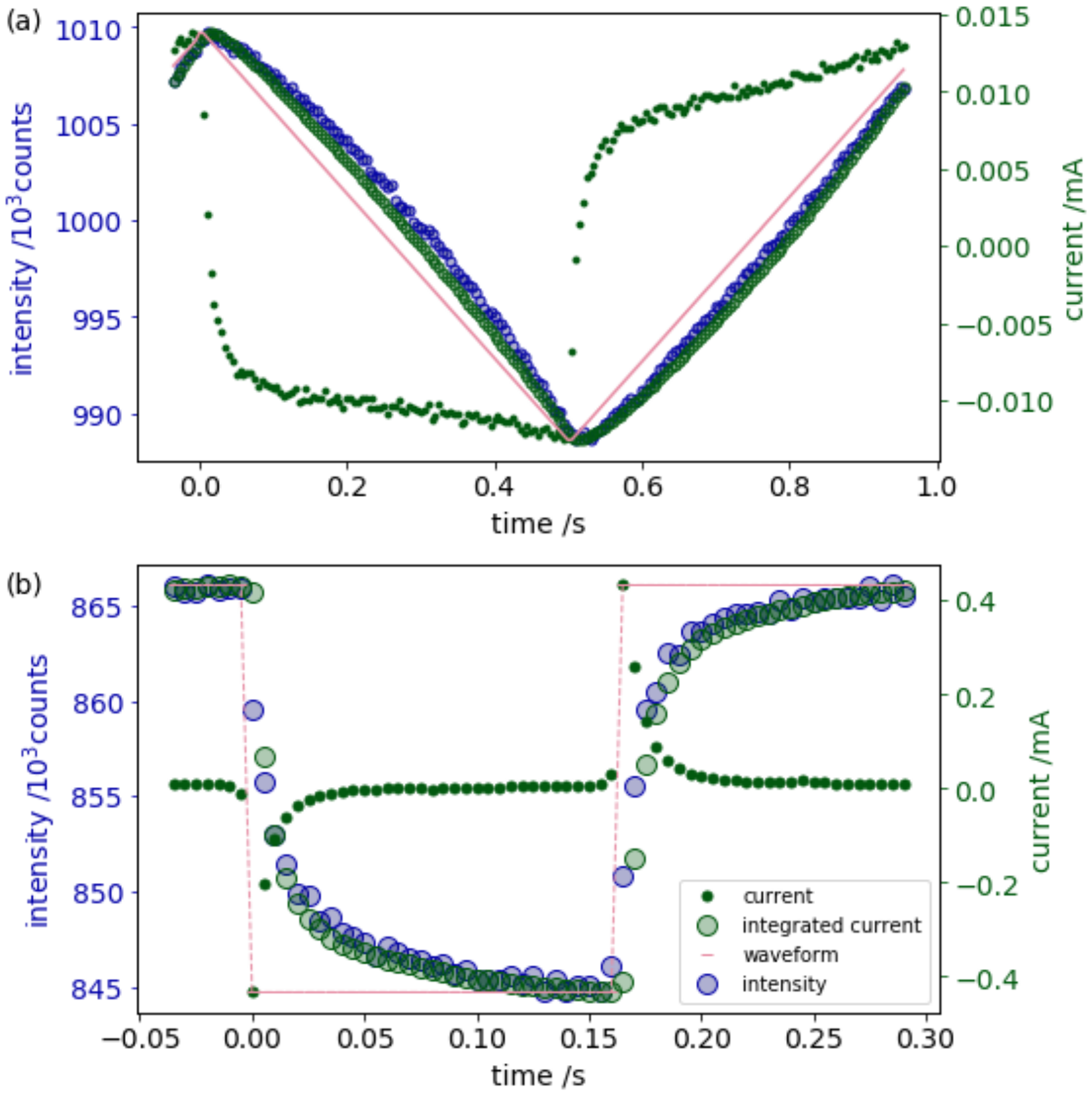

Figure 24: The optical signal from the EDL under variable surface potentials. For resp. (a) and (b) a triangular and square waveform between −1 and +1 V plotted in pink, with in blue circles the optical signal, in green dots the current and in green circles the integrated current. Both the integrated current and optical signal show exponential decay with a decay time that corresponds to the charging time of the electro-chemical cell as a capacitor. The sample was an ITO grain in 10 mM NaCl solution.

In our experiment there are many physical effects going on that could be responsible for what we see, but

many of them would have completely different timescales. So the timescales of what we measure can tell us more about the origin of it. Our measurements of this timescale are shown in figure 24.

Since we predict that the optical contrast we see depends on the EDL we would expect the timescales to be the same as the timescale at which the EDL changes. When applying an electrical potential over our cell it will behave as a capacitor. It will gather ion charges around its electrodes to screen the applied potential inside the liquid. This is essentially the same as what the electrical double layer is, a screening layer for the bulk from a charge. The formation of this capacitor charge in our cell can be measured by looking at the current trough the sample, where the integrated current would be equivalent to the amount of charge in the form of ions gathered at the electrode surface. Figure 24b clearly shows the timescale of the integrated current and intensity matches.

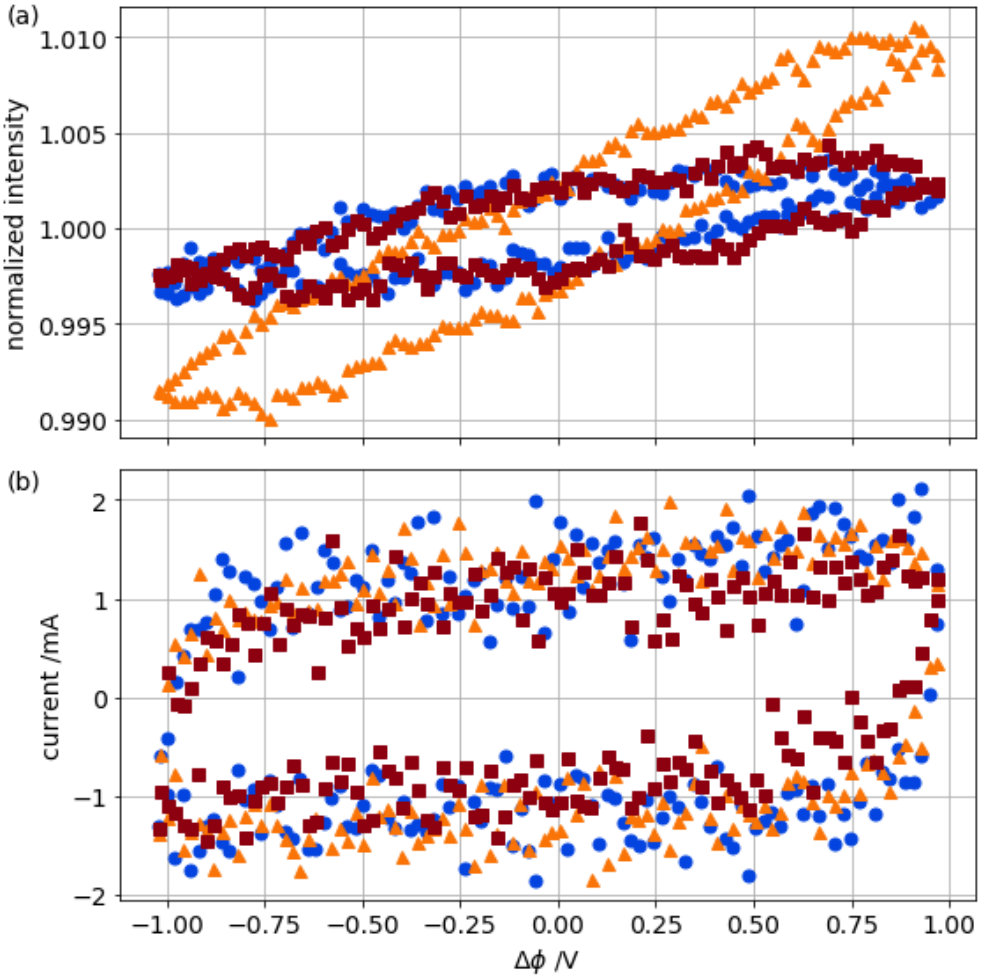

Figure 25: The potentiodynamic optical contrast (a) and the cyclic voltagram (b) for the same ITO grain for three different salts. The measured salts are NaCl (blue circles), NaBr (red squares) and NaI (orange triangles) all at a concentration of 10 mM and the measurements are all taken at 1 Hz.

When measuring the potentiodynamic optical contrast (PDOC) for different types of salt we find a dependence on the type of salt. In figure 25 we see that the intensity variation is significantly larger for NaI

compared to the other salts. When seeing that the intensity variation changes scale depending on salt but the current is the same regardless of the salt we can only be explain this based on our theory of the optical contrast being caused by the change in the EDL.

In our prediction, section 2.8, we have linked the PDOC to the factor K which is the factor between saltwater polarizability change and salt concentration. The optical polarizability of NaI is larger than that of NaCl and NaBr, so the difference is predicted and scales the correct way. However the optical contrast seen from NaCl and NaBr seems the same while their optical polarizability is not. We do not know why we do not see this difference, it can be that we did not have a high enough accuracy in our measurements yet.

7.2 Deposited chromium particles

Waiting for colloidal particles to land like in section 5.2.2 is not the only technique for depositing particles. In this experiment I analyse a sample where chromium was deposited using physical vapor deposition.

Since I was not personally involved with making the sample I cannot go into detail on the sample but I will explain what it is. The sample used for this measurement had chromium deposited, which probably oxidized when in contact with the water in the sample. Being made with physical vapor deposition the sample could be made with more control over the result, with a spatial filter the chromium in the sample was only deposited at spots in a triangular lattice with $4.5\mu m$ spacing.

In figure 26 a figure of the sample with chromium deposited is shown with various locations annotated. The points from 5 to 16, except 7, are the deposited chromium because their spacing is in a triangular lattice with the correct distance. The other points are dirt particles or more pronounced ITO grains.

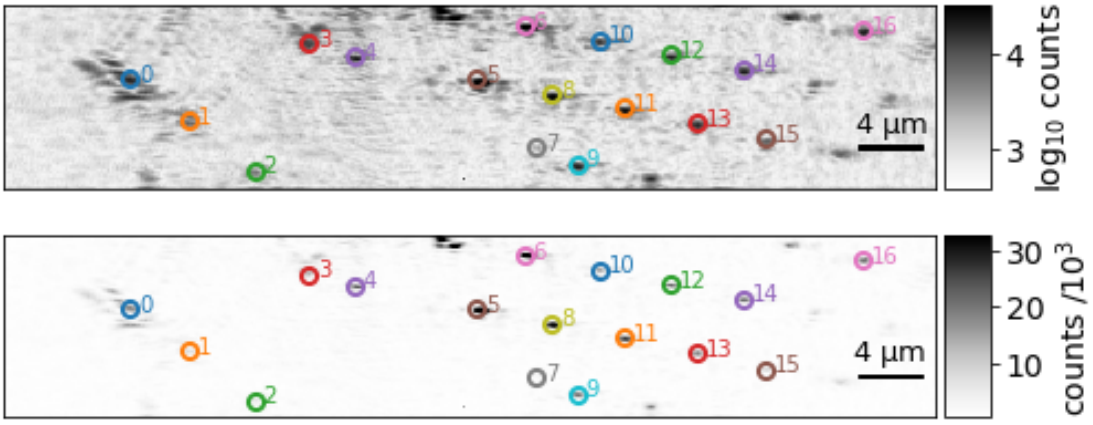

Figure 26: Image of the sample with chromium deposited, shown in $\log_{10}$ counts and raw counts. The annotated spots are analysed further.

With more measurements with a similar amount of interesting features to look at this could have been very work intensive. To make this easier I wrote a special analysis file where it was possible to chose many points and analyse them individually but automatically. I only had to click once near every feature to analyse all of them.

The results of analysing all the annotated features in figure 26 is shown in figure 27. As mentioned before the points 5 to 16, except 7, are the deposited chromium and in this measurement these are the particles that show similar behavior. Their intensities behave mostly linear and negatively correlated with potential. The other particles have intensities that are often not really linear and sometimes not negatively correlated with potential. This observation is not without exceptions, but it is consistent enough to look further into.

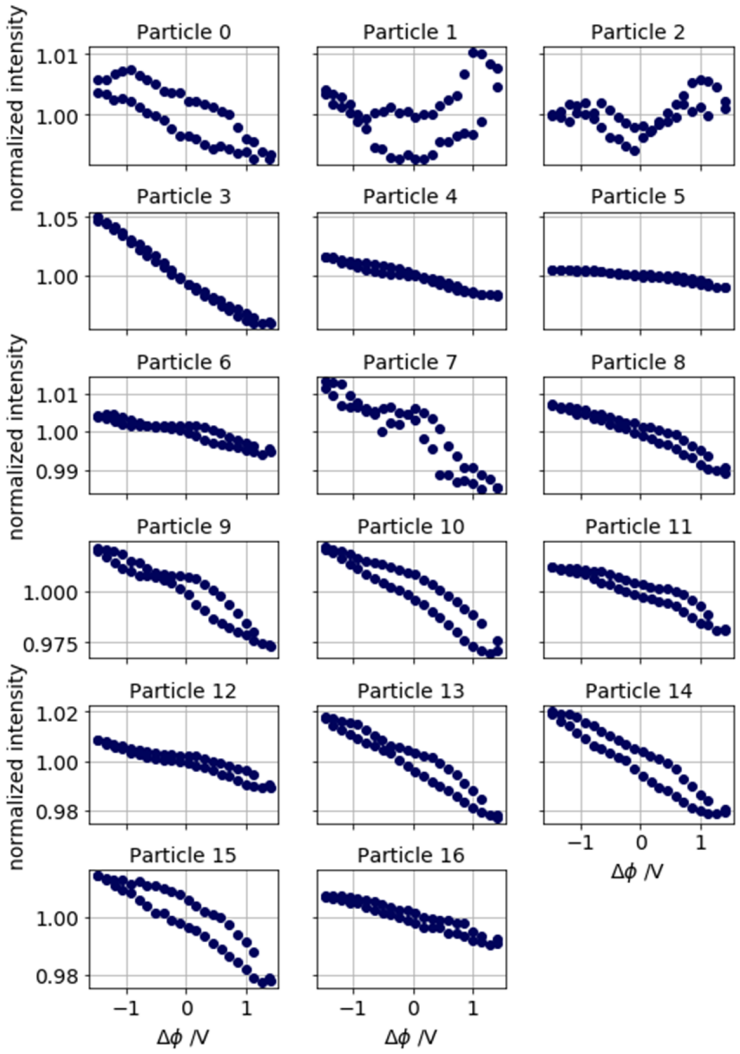

Figure 27: The normalized intensity versus the applied potential for the particles annotated in figure 26.

We know of a few reasons why the behavior of the features in figure 27 is not completely consistent. The illumination is not perfectly homogeneous spatially, this is a known limitation of the setup in its current state. Also the particles might have different sizes and shapes which can influence the relative intensity change due to the applied potential. Lastly the dirt or ITO grains in the image can vary a lot and could be chromium that broke off somewhere else, which causes it to have the same behavior as the chromium deposits on the right spots.

We have looked at the correlation between each pixel in the image in time with two typical particles' intensities in time, this is seen in figure 28. The particle chosen for correlation in (b) has a intensity in time that was very similar to the typical intensity in time of the identified chromium particles. These chromium particles indeed do seem to correlate strong enough with the chosen particle to be clearly visible in this figure. The correlation of the chromium particles is however hardly visible for the figure with the correlation with the particle chosen in (c) that has a intensity that is more consistent with the typical ITO intensity in time.

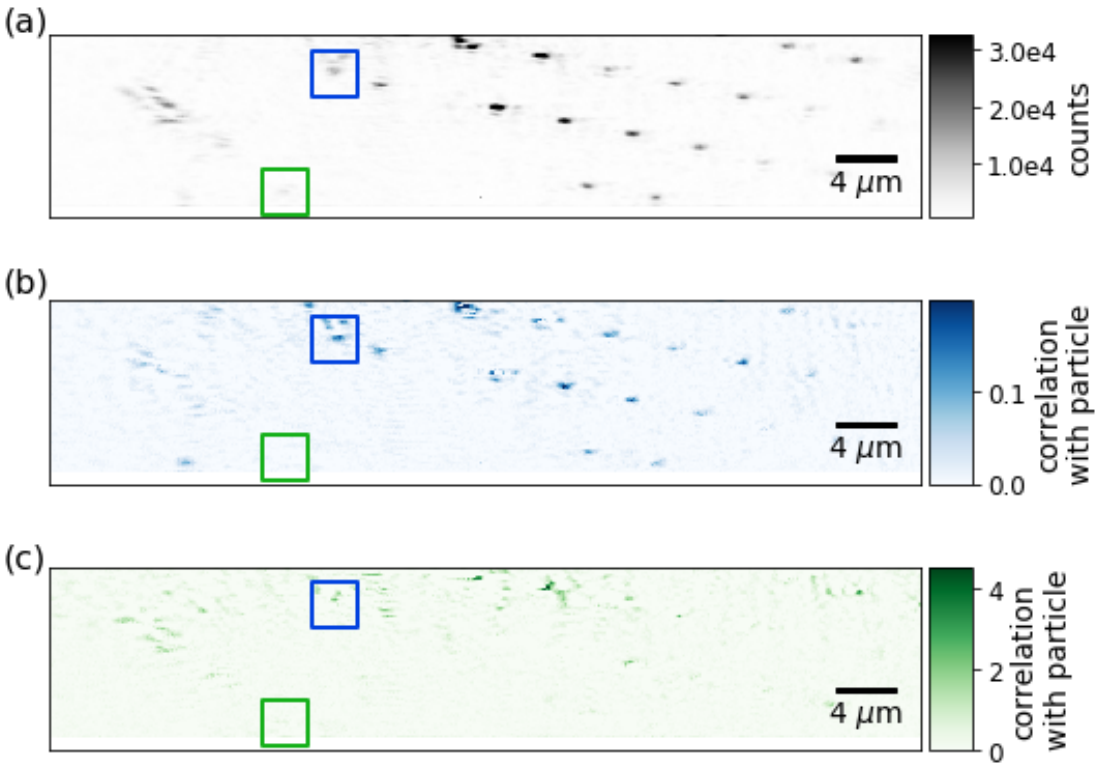

Figure 28: The (a) image of the sample with chromium deposited, (b) correlation with the blue spot in time and (c) correlation with the green spot in time. The blue and green spot are annotated with a square of the resp. color in (a), (b) and (c). The blue and green spot are also resp. particle 2 and particle 3 from figure 26 and 27. The correlation that is plotted is calculated as the average over all cycles for the covariance between the position and the chosen particle divided by the variance of the position.

7.3 Varied offset potentiodynamic optical contrast

In figure 23 we see a change in the behavior of the PDOC at higher applied potentials. The red curve gets more flat at higher positive applied potentials. This could indicate that some chemical reactions start happening which change the contents of the EDL and therefor how the PDOC behaves. To get a better idea what is happening at different potentials we will do low amplitude scans at different potential offsets.

The low amplitude scans allow us to find the slope of the PDOC around the used offset. Low amplitude scans are not influenced by chemical reactions that start happening outside of their range, which can influence a full scan when the chemical reaction has a long relaxation time. For example if a reaction causes bubbles to form, these might not disappear before the full measurement is far away from a potential where these are created.

We can find the slope the PDOC makes at each offset and plot this slope vs the offset. The resulting plot should give an insight in the behavior of the sample dependent of offset.

The potential we apply for varied offset PDOC is shown in figure 29. We apply a 10 Hz, 0.25 V amplitude potential at different voltage offsets in succession, where we can repeat the cycle over different offsets many times. For each new offset we wait a few cycles for the system to find a sort of equilibrium before using it

in analysis.

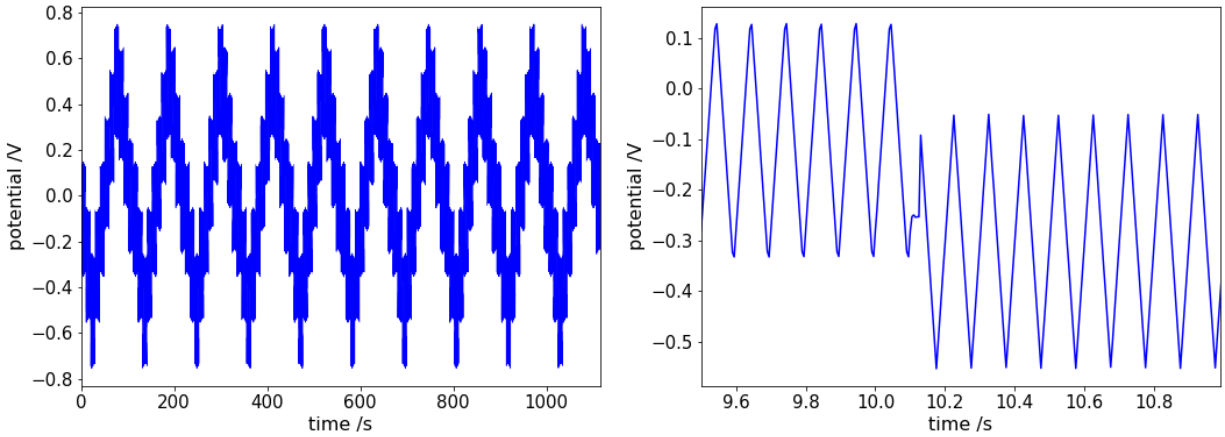

Figure 29: The applied potential for varied offset PDOC, with on the left the full measurement and on the right a cutout. The potential is always a 10 Hz wave with approximately 0.25 V amplitude, with its offset cycling between -0.5 and 0.5 V in small steps changing every 10 seconds.

To analyze the effects of the varying offset we select a particle and for each offset we plot the slope of the normalized PDOC. This results in a plot of PDOC slope versus offset that we expect to be a measure of the activity of reactions in the EDL. For the potential shown in figure 29 we expect a constant slope versus the offset because these low potentials do not introduce large reactions as far as we know.

We did this experiment in an ITO flowcell without introduced particles and with a salt solution of 0.1 M NaI. The result for an ITO grain is plotted in figure 30.

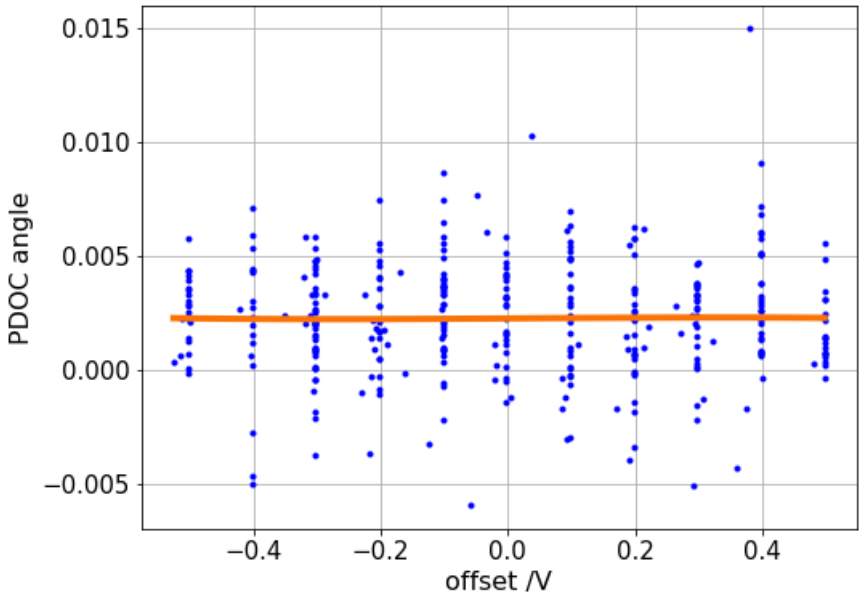

Figure 30: The slope of the PDOC for various offsets (blue) and a 3rd order polynomial fit (orange). Data from an ITO grain in 0.1 M NaI salt solution.

In figure 30 the constant slope of the PDOC we expected was indeed found. The spread of the slope of the PDOC is quite large for every offset, so the large quantity of measurements was and probably is needed for all of these measurements.

With the value of the slope of the PDOC at low offsets known we can try to do this for offsets of which we do not know for certain what to expect. With the same type of sample I repeated the measurement with larger offsets in potential, seen in figure 31.

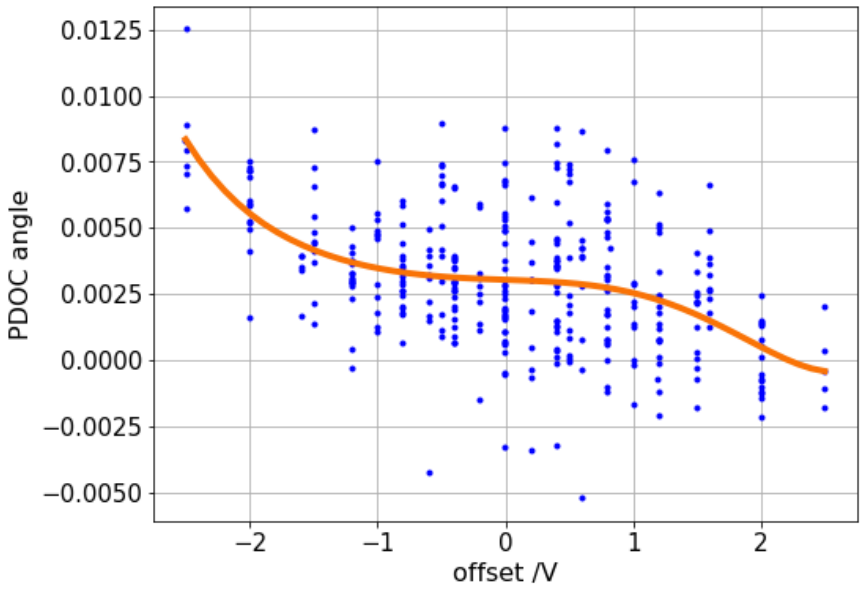

Figure 31: The slope of the PDOC for various offsets (blue) and a 6th order polynomial (orange). Data from an ITO grain in 0.1 M NaI salt solution.

To show how this translates to a PDOC we can integrate it, see figure 32. This recreated PDOC has a shape that passes for a real measurement on an ITO grain over a similar potential range, seen in figure 23.

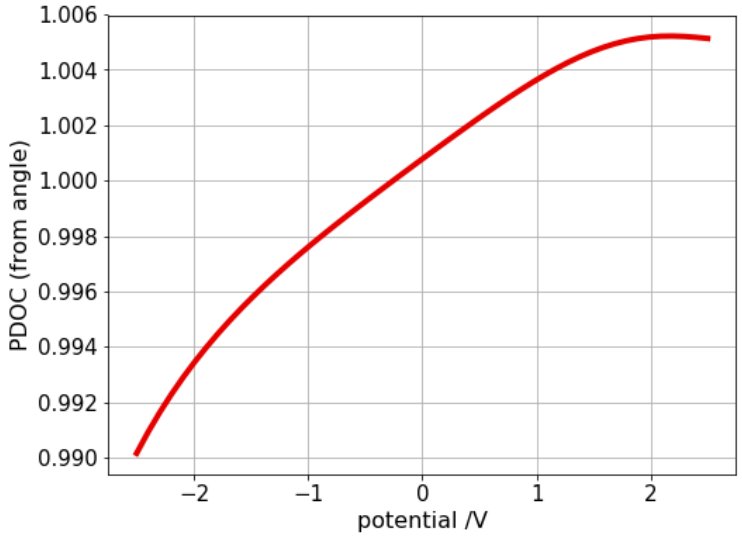

Figure 32: The PDOC as found by integrating the slope of the PDOC found in figure 31 and translating to a variation around the mean.

8 Discussion

In this section I will discuss all the results from section 7 and speculate on future possibilities with the techniques presented here.

8.1 Intensity change due to the electric double layer

I had the hypothesis: "We find intensity variations proportional to the applied potential that we can best explain due to the electric double layer."

I think section 7 has supported this hypothesis enough. While the result in figure 25, on the dependence of ion type, still has some mysteries, I personally find figure 24, on the timescales, already quite convincing. The timescale we see is connected to the timescale of the cell's capacitor type charging, which is physically explained by exactly the same mechanism as we claim our PDOC comes from: the changing of the EDL. Most other timescales differ in orders of magnitudes and we have seen this timescale being the same for measurements with many different parameters, so even if it just happened to be the same once it is very in-probable to have been the same every time.

8.2 Deposited chromium particles

This measurement shows that similar particles have similar behavior in intensity change depending on applied potential. We are interested in this because this shows that our results are consistent between particles of the same material, which is required for making use of the spatial possibilities of this type of setup.

Another possible use of looking at correlation can be that particles that are otherwise not distinguishable from background can be identified by their optical behavior under a potential. This would already be quite useful but a possible application in the far future could be a similar technique of labeling with fluorescent particles with specific correlating particles or even the correlation of the to be labeled substance itself.

8.3 Varied offset potentiodynamic optical contrast

The first results of this method were from measurements where the parameters for the offsets en amplitude where taken with large safety margins. These margins were taken to be sure the sample did not physically change during the more extreme measurements of over $\pm$1V, thereby changing the other results as well.

Of this measurement we could expect a constant value for the slope of the PDOC and it is nice to have predicted this correctly, but this is not a result that was very insightful. For an insightful result we need to go to higher offsets and hope to find a change in the slope at some point.

In the second measurement, figure 31, we find the same constant slope of the the PDOC as in the previous experiment, but new behavior at larger offsets from 0. The data in figure 23 already showed a flatter shape of the PDOC at high values of the potential. This is also seen in figure 31, as for high positive offsets the slope becomes less. For high negative potentials the slope of the PDOC seems to become larger. We have not clearly seen this feature in measurements of the PDOC with a single wave.

These features might both be caused by the electrolysis of water becoming more probable at higher potentials.

This technique of varied offset PDOC is up to now the most accurate technique we have used, but it also has had the most data points. Varied offset PDOC has results that are consistent with all other results and has one of the best accuracies. But its measurements take a lot of data points, more than other measurements usually take. This large amount of data might be the main reason it is quite accurate.

The advantage of varied offset PDOC should be that it can have more accuracy in at what potential new behavior of the PDOC starts, because relaxation times are no longer an issue when the activation of reactions is not even reached. However with the current setup it is not the accuracy in potential but mechanical drift

that is the main limitation. With an improved setup it is possible that this technique can distinguish itself better.

8.4 Compared to other potentiodynamic techniques

The potentiodynamic optical contrast mechanism in this thesis is a new way of looking at potentiodynamic phenomenon. Here I want to compare it to existing techniques and argue for its usefulness.

Industry will often require certain (chemical) reactions to happen as efficient as possible, so learning more about reactions is home to large fields of study. One important direction of such studies is the study of voltammetry, an electroanalytical method that gathers information from the current running through a sample as the potential is varied.

Voltammetry, section 2.7, relates to our measurements because we essentially do the same, we also look at variations caused by potential. In voltammetry the current variations caused by potential give information on the types of molecules in the sample or the activation energy needed for reactions. On the other hand with PDOC we look at intensity changes of single particles. While we right now do not have the accuracy of established voltammetry techniques, our technique does potentially give new insights with its ability to see single particles, possibly even in non homogeneous mixtures. Our technique can borrow a lot from voltammetry, both from relating to the results and from the technique itself.

We can learn a lot from how voltammetry applies potentials. There is a lot known about at what scanrate (volts per second) we should do measurements. This scanrate should be slow enough that the size of the background currents is small enough to identify the peak from any reaction happening[13]. A low scanrate will however cause a lower peak, which at some point becomes lower than our noise. There are also different ways of applying a potential that can have advantages like more precision in potential. For example with a small amplitude triangle wave where the offset it changed, this we have already tried after being inspired by voltammetry.

The potentiodynamic optical contrast will initially not have the robustness and accuracy of the existing voltammetry experiments, but its ability to do measurements on single particles that can be spatially distinguished is promising.

8.5 Outlook

Since with PDOC it is quite new that we see optical contrast based on applied potential there are a lot of possibilities for the future of this work.

The supporting theory for this technique is also quite new and therefor it is possible it might not be the best explanation. Since there are still some mysteries regarding figure 25 it probable we are not yet aware of everything that is happening inside the sample. This might make it seem like we do not support our current theory, but we do support it. Current data is best explained with the theory as described in section 2.8.

While I have made comparisons between PDOC and voltammetry in this thesis, it is not the same on a quite fundamental level. The light we see is influenced by the changes to refractive index in the liquid and only because this refractive index depends on ion concentration, which is related to capacitance and therefor electric currents, are PDOC and voltammetry related. Because of the fundamental difference between the techniques there will be different limitations to what is possible and we do not know the limitations of PDOC yet.

Currently we have known limitations in our setup, but we also have solutions. The limitations are that the ITO we use is known to not be chemically inert at higher potentials [12] and that the high stability we require for measurements is barely reached in some measurements. If available transparent conductive materials like ITO do prove to be too chemically reactive it is perhaps possible to use thin wires or graphene in some configuration where the EDL is still visible. And small improvements to mechanical stability will

probably be enough because the current setup can already image small details of the PDOC while having clear limitations to its performance in mechanical stability.

A simple way of improving our findings is making a better setup because we currently have significant noise caused by the instability of the setup. This is already being worked on in the group: a second setup is being made with improvements to stability.

To gain an accurate knowledge of the chemical limitation we will need to use a reference electrode[13], this is difficult to place in our setup but necessary for finding these limitations in a correctly calibrated way. We already have some contacts that are helping with the possible problems with ITO being chemically active in our setup.

Because PDOC is sensitive to the ion concentration it might be possible to measure spatial information about the flow or diffusion of liquid with different ion contents. Right now this is an empty claim, as we have not tried this or seen anything suggesting this. It is however among the possibilities we can consider when thinking of other uses for this technique.

References

[1]C. Jing and J. Reichert, "Nanoscale electrochemistry in the "dark-field"", Current Opinion in Electrochemistry **6**, 10–16 (2017).

[2]C. P. Byers, B. S. Hoener, W.-S. Chang, S. Link, and C. F. Landes, "Single-particle plasmon voltammetry (sppv) for detecting anion adsorption", Nano Letters **16**, PMID: 27006995, 2314–2321 (2016).

[3]M. E. Snowden, A. G. Güell, S. C. S. Lai, K. McKelvey, N. Ebejer, M. A. O'Connell, A. W. Colburn, and P. R. Unwin, "Scanning electrochemical cell microscopy: theory and experiment for quantitative high resolution spatially-resolved voltammetry and simultaneous ion-conductance measurements", Analytical Chemistry **84**, PMID: 22279955, 2483–2491 (2012).

[4]R. Parsons, "The electrical double layer: recent experimental and theoretical developments", Chemical Reviews **90**, 813–826 (1990).

[5]LEMI (MIT), *Schematic of the electrical double layer*, Website: http://web.mit.edu/lemi/rsc_electrokinetics.html.

[6]D. Griffiths, *Introduction to electrodynamics*, 3rd, ISBN 81-7758-293-3 (Pearson Education, Dorling Kindersley, 2007) Chap. Chapter 4.

[7]W. Heller, "Remarks on refractive index mixture rules", The Journal of Physical Chemistry **69**, 1123–1129 (1965).

[8]P. V. Rysselberghe, "Remarks concerning the clausius-mossotti law", The Journal of Physical Chemistry **36**, 1152–1155 (1932).

[9]N. An, B. Zhuang, M. Li, Y. Lu, and Z.-G. Wang, "Combined theoretical and experimental study of refractive indices of water–acetonitrile–salt systems", The Journal of Physical Chemistry B **119**, PMID: 26203663, 10701–10709 (2015).

[10]J. H. Seinfeld and S. N. Pandis, *Atmospheric chemistry and physics*, 2nd, ISBN 0471720186 (John Wiley and Sons, 2006) Chap. Chapter 15.1.1.

[11]D. J. Griffiths and D. F. Schroeter, *Introduction to quantum mechanics*, page 62, 2nd (Cambridge University Press, 2018).

[12]E. Matveeva, "Electrochemistry of the indium-tin oxide electrode in 1 M NaOH electrolyte", Journal of The Electrochemical Society **152** (2005).

[13]N. Elgrishi, K. J. Rountree, B. D. McCarthy, E. S. Rountree, T. T. Eisenhart, and J. L. Dempsey, "A practical beginner's guide to cyclic voltammetry", Journal of Chemical Education **95**, 197–206 (2018).

[14]K. Namink, X. Meng, M. T. M. Koper, P. Kukura, and S. Faez, *Optical imaging of the electric double layer around nanostructures*, 2019.

[15]W. P. Ambrose, P. M. Goodwin, and J. P. Nolan, "Single-molecule detection with total internal reflection excitation: comparing signal-to-background and total signals in different geometries", Cytometry **36**, 224–231 (1999).

[16]T. J. F. Stephen T. Ross Stanley Schwartz and M. W. Davidson, *Total internal reflection fluorescence (TIRF) microscopy*, Website: microscopyu.com.

[17]G. F. Franklin, J. D. Powell, and A. Emami-Naeini, *Feedback control of dynamic systems*, 7th (Prentice Hall Press, Upper Saddle River, NJ, USA, 2014).

[18]E. Fortunato, D. Ginley, H. Hosono, and D. C. Paine, "Transparent conducting oxides for photovoltaics", MRS Bulletin **32**, 242–247 (2007).

[19]Hamamatsu, *Orca-flash4.0 v3 technical note* (2018).

[20]G. Kavei, Y. Zare, and A. Mohammadi Gheidari, "Evaluation of surface roughness and nanostructure of indium tin oxide (ITO) films by atomic force microscopy", Scanning **30**, 232–239 (2008).

[21]G. Sitterley, "Poly-lysine", BioFiles **3**, 12 (2008).

[22]D. Allan, C. van der Wel, N. Keim, T. A. Caswell, D. Wieker, R. Verweij, C. Reid, Thierry, L. Grueter, K. Ramos, apiszcz, zoeith, R. W. Perry, F. Boulogne, P. Sinha, pfigliozzi, N. Bruot, L. Uieda, J. Katins, H. Mary, and A. Ahmadia, *Trackpy*, 10.5281/zenodo.3492186, Oct. 2019.

[23]uetke and K. Namink, *UUTrack*, GitHub, github.com/uetke/UUTrack, Nov. 2019.

[24]K. Namink and S. Faez, *PDSM package*, UU gitlab, git.science.uu.nl/linx/PDSM, possibly requires a request for access, 2019.

A List of materials

Below are the materials we used listed:

Laser	Laser Quantum IGNIS 660nm 400mW Red DPSS
Camera	Hamamatsu Flash v4.0 [19]
QPD	Thorlabs PDQ80A
Objective	A high NA oil immersion objective of around 100x magnification
Lens	Thorlabs LA 1027 plano convex f=35mm
Lens	Thorlabs LA 1433-A plano convex f=150mm
Lens	Thorlabs LA 1433 plano convex f=150mm
Lens	Thorlabs LA 1433 plano convex f=150mm
Lens	Thorlabs LA 1509-A plano convex f=100mm
Lens	Thorlabs LA 1761-A-ML Coating 350-700nm f=25mm
Mirrors	Thorlabs
Optical cage system	All pieces from Thorlabs

Table 1: Materials used for the microscope.

In table 1 most of the hardware for the optical system of the setup is shown. What might be interesting from this list is that most is bought from Thorlabs, which is a supplier of high quality but quite expensive lab equipment.

The camera was water cooled using an unknown water cooler that required a home made power source connection. The model is no longer in production.

Piëzo controller	Thorlabs Kinesis KPZ101 K-cube
Position Sensing Detector	Thorlabs Kinesis KPA101 K-cube
QPD signal to PID loop thing	Thorlabs PDQ80A
Digital-analogue converter	NI DAQ 6212 BUS
Programmable wave generator	Agilent 33120A

Table 2: External electronics used in the setup. The DAQ is used for multiple purposes: wave generation and data logging.

Table 2 shows the hardware for most of the electrical system in the setup. The QPD signal is translated to new voltages for the piëzo to keep the setup in focus. The DAQ is used for various things, see chapter 4.4 and 4.5.

ITO slide	Diamond Coatings, 70 - 100 Ohms/Sq.
ITO slide cover	ITO flexible plate
Flow-cell walls	dual sided sticky tape
Wires	insulated copper wire

Table 3: Materials used for the sample.

For how the sample is made using these materials see section 4.7.

Microscope GUI (Guided User Interface)	modified UUTrack[23]
Piëzo controller	APT controller

Table 4: Software we use.

For more information on UUTrack see section 4.8 and appendix B.

APT controller is a program supplied by the manufacturers of the Thorlabs Kinesis cubes that can be used to change their settings from the computer. We prefer to change them from the computer because navigating the settings is much easier with mouse and keyboard.

B UUTrack code

UUTrack is a python package created at nanoLinx as a GUI (Guided User Interface) for experimental setup cameras. It shows a preview and helps start and stop measuring.

I'll go trough the filestructure and explain what is in what folder with occasionally more information on certain files.

The documented version of UUTrack in this document is this experiments very own dedicated branch of the UUTrack software. Because it branched when the UUTrack software was using the now outdated PyQt4 package instead of the updated PyQt5. Because PyQt4 has some compatibility issues it possibly requires some tricks to get our version of UUTrack running. These tricks would be gladly learned of if they are found out, because right now it is up to whomever wants to use it to solve these issues. So to be clear: there are probably unknown issues that will making a fresh install hard.

B.1 Data generated by UUTrack

When finishing a measurement with UUTrack you have a number of `"(..).hdf5"` and `"(..)_m#.npy"` files, where `(..)` is what you called the measurement. These files you can analyze using the file `"PDSM/Analysis/data_processing/new_analysis_file.py"`. This analysis file imports the data, identifies some properties of the data, helps you select a particle of interest, applies drift correction, averages over cycles and plots various possibly interesting sets of data. Among the final plots are intensity versus time and intensity versus applied potential.

This analysis file starts with a part containing some settings that speak for themselves and then there are various blocks doing the steps for analysis. Each block starts with a very short explanation what it does and how to use it. While executing a block it will show some preliminary results, that sometimes help you find the best settings.

B.2 UUTrack dependencies

Python 3.6 with the following packages:

```
alabaster==0.7.10
argh==0.26.2
Babel==2.4.0
cffi==1.11.5
colorama==0.3.7
cycler==0.10.0
docutils==0.13.1
h5py==2.8.0
imagesize==1.1.0
Jinja2==2.9.5
kiwisolver==1.0.1
Lantz==0.3
livereload==2.6.0
MarkupSafe==1.0
matplotlib==3.0.2
numpy==1.15.4
olefile==0.46
pathtools==0.1.2
Pillow==5.3.0
Pint==0.8.1
pip==18.1
```

```
port-for==0.4
psutil==5.4.8
pycparser==2.19
PyDAQmx==1.4.2
Pygments==2.2.0
PyOpenGL==3.1.0
pyparsing==2.3.0
PyQt4==4.11.4
pyqtgraph==0.10.0
python-dateutil==2.7.5
pytz==2018.7
PyVISA==1.9.1
PyYAML==3.13
requests==2.13.0
scipy==1.1.0
setuptools==40.6.2
six==1.11.0
snowballstemmer==1.2.1
stringparser==0.4.1
tornado==4.4.3
watchdog==0.9.0
wheel==0.32.3
```

Like mentioned before, when using a fresh install it is quite possible there are difficult to install packages.

B.3 /PDSMGUI

This `/Config` folder holds the used configuration files.

There are various text and code files that speak for themselves. The `startProgram.py` file is called with python to start the software.

The folder `/UUTrack` holds this setups highly edited version of UUTrack and is documented in the coming subsections.

B.4 /UUTrack

`startMonitor.py` is important as code. It is the code that actually starts the software and when changing cameras it is quite possible that this code needs to be edited apart from the configuration file because it is slightly hard coded.
`DAQwavegeneration.py` is a seperate program to use the DAQ as a wavegenerator. Usefull as a reference for writing new code with the DAQ, however not all code inside it work.

B.5 /UUTrack/Controller/devices

In each folder here there is the basic initial interface for using different camera's with the python program. The Hamamatsu is definitely working, the Basler is probably working and the rest has not been checked.

B.6 /UUTrack/Model

Holds the code for saving data from the camera, correctly communicating with the camera and the code for remembering, using and loading the settings set in the UUTrack program.

B.7 /UUTrack/Model/Cameras

This folder holds the python files which 'represent' the possible cameras the program can use. They should work if the required files in the devices folder (section B.5) are working correctly. The name of these files is used when configuring what camera to use if you want to change the used camera in the code, some cameras will not be possible to change to using the config file without changing the code in various places.

B.8 /UUTrack/View

The `hdfloader.py` can be very useful when taking a look at the created data and the `/Monitor` folder (section B.9) holds a lot of code which will be the next section.

B.9 /UUTrack/View/Monitor

This is the big one. With all the behind the scenes stuff out of the way, the code here will directly appear on screen when running the files. I will go trough each file quickly because it is reasonably commented.

Icons A folder with all icons used in `monitorMain.py`.

LocateParticle.py Currently unused code, kept here because it might be useful in the future. The LocateParticle class contains necessary methods for localizing the centroid of a particle and following its track.

NIcontrol.py File with a class used to communicate with the NI DAQ (section 4.4) correctly for this setup. It sends the commands to start and stop to measure all required channels with the camera as a trigger and to first flash a LED to synchronize the data. It also holds the code for generating waves with varying offset with the DAQ from the UUTrack GUI.

cameraViewer.py Currently unused code, it is supposed to start an extra window which only shows the current camera image. Kept here because it might be useful in the future.

clearQueueThread.py This file holds a class that clears the queue from the "QtCore.QThread", I think it is not used. I expect it to have been useful when debugging and might be in the future.

configWidget.py This file creates the "Parameters" tile/widget in the main window. This widget can be used to view and change the settings that have been set in the config file supplied when starting the program.

contrastViewer.py Creates a window that displays a 1D plot of a cross cut on the main window. It is currently unused.

crossCut.py Plots total intensity value of line trough image while taking background corrections into account. Its functional but not useful in practice.

mainImageManipulation.py Holds a class that manipulates the mean image seen in the GUI. Is required to correctly use binning and the various background correction methods for the GUI. Any change it makes to the image shown in the GUI is NOT saved when recording data.

messageWidget.py Is used to create "Messages" tile/widget in the main window. It shows a permanent message for every important action done by the user in a log style and it shows the status of some parameters from the camera and measurement.

monitorMain.py This is a very large file which is responsible for creating the main window with all its widgets. It has all the code necessary to use the various widgets from the different python files in this folder and to make this as easy to use as possible there is also a lot of code concerning shortcuts and menu bars. Because of the length of the `monitorMain.py` file you might think it does a lot of calculations as well, but this is almost all done in the different imported files it calls from.

monitorMainWidget.py This file holds the code responsible for the large preview of the camera image in the main window. This window shows what the camera can currently see and it is possible to change the range of interest in this widget. There is also the possibility to plot the intensity at a certain location in the plot by pressing alt while hovering over the image, this is a feature that is not recommended for use but can be expanded on in the future.

popOut.py Creates a pop-out window class that can be used to show information. Is currently only used to create a pop-out that shows all the keyboard shortcuts available.

resources.py This is "resource object code". It is probably important.

specialTaskTrack.py Similar to the "UUTrack.View.Camera.workerThread", the special task worker is designed for running in a separate thread a task other than just acquiring from the camera. For example, one can use this to activate some feedback loop. This is unused code but has been used as a reference for how to write other code. When implementing some sort of particle tracking this might be a useful file, so it is kept.

specleWidget_space.py Creates a new window that shows the (spatial) variance of the speckle pattern in the center of the current ROI in the image over time and some parameters like the amount of oversaturated pixels in the image. Interchangeable with the `specleWidget_time.py` file, which is thought to be more useful.

specleWidget_time.py Creates a new window that shows the average deviation of pixel intensity in time by showing the average of normalized variation for a few frames of different pixels at different starting times. It also shows some parameters like the amount of oversaturated pixels in the image. Interchangeable with the `specleWidget_space.py` file, but this one is probably more useful.

trajectoryWidget.py Creates a widget in the main window to plot the intensity of a pixel selected by holding alt and hovering over the preview image in the GUI. It is not very useful as it is right now but for potential future uses it is kept.

waterfallWidget.py A not very useful, but functional, widget that plots a waterfall plot. Perhaps can be changed to something else in the future.

workerThread.py Contains a thread class that acquires continuously data until a variable is changed. This enables to acquire at any frame rate without freezing the GUI or overloading it with data being acquired too fast.

C Data analysis code

I have written a lot of data analysis code, available here [24]. In this appendix I will describe some of the analysis files that can be found in this package.

The code is approximately structured as follows: a `data_processing` folder with various files that can be edited to analyse the data in various ways and a folder `PDSM_func` folder with files holding code that is used by the files in the former folder to do the analysis. This way it is possible to make improvements to various functions and having them applied to all analysis files without having to edit them all.

C.1 DFSM.py

Many analysis files rely heavily on a secondary file that has many of our functions in it. This secondary file is this file, found at `/PDSM/Analysis/PDSM_func/DFSM.py`.

There are two parts to this file: first a part regarding importing data files, which was mostly written by other people, and secondly a part containing many functions doing calculations for other analysis files to use. By keeping this in a secondary file to be imported improvements to the code are almost always backwards compatible. The functions are commented reasonably well and are more or less in the order they are called when analyzing.

C.2 new analysis file.py

The aptly named `new_analysis_file.py` holds the standard way of analysing data. It can be found in `/PDSM/Analysis/data_processing/`. After copying and renaming the file you only need to edit a few lines to make it import and analyze the new data.

It creates the graphs as described in section 6.5 and during the data processing process it reports on what it has done with various graphs, so if it doesn't automatically do the right thing you will be able to notice it.

C.3 LandingCheck.py

The `LandingCheck.py` file can find the particles landing in a movie. It can be found in `/PDSM/Analysis/data_processing/`.

There are a few important parameters that can be quite different for binned or less brightly illuminated movies, so it might take some getting used to. This file uses the python package trackpy [22]. Reading up on this package will help find the correct settings.

This file filters for only landing particles by the fact that a certain background correction method, section 5.2.2, will create a particular signal in intensity that can be selected for.